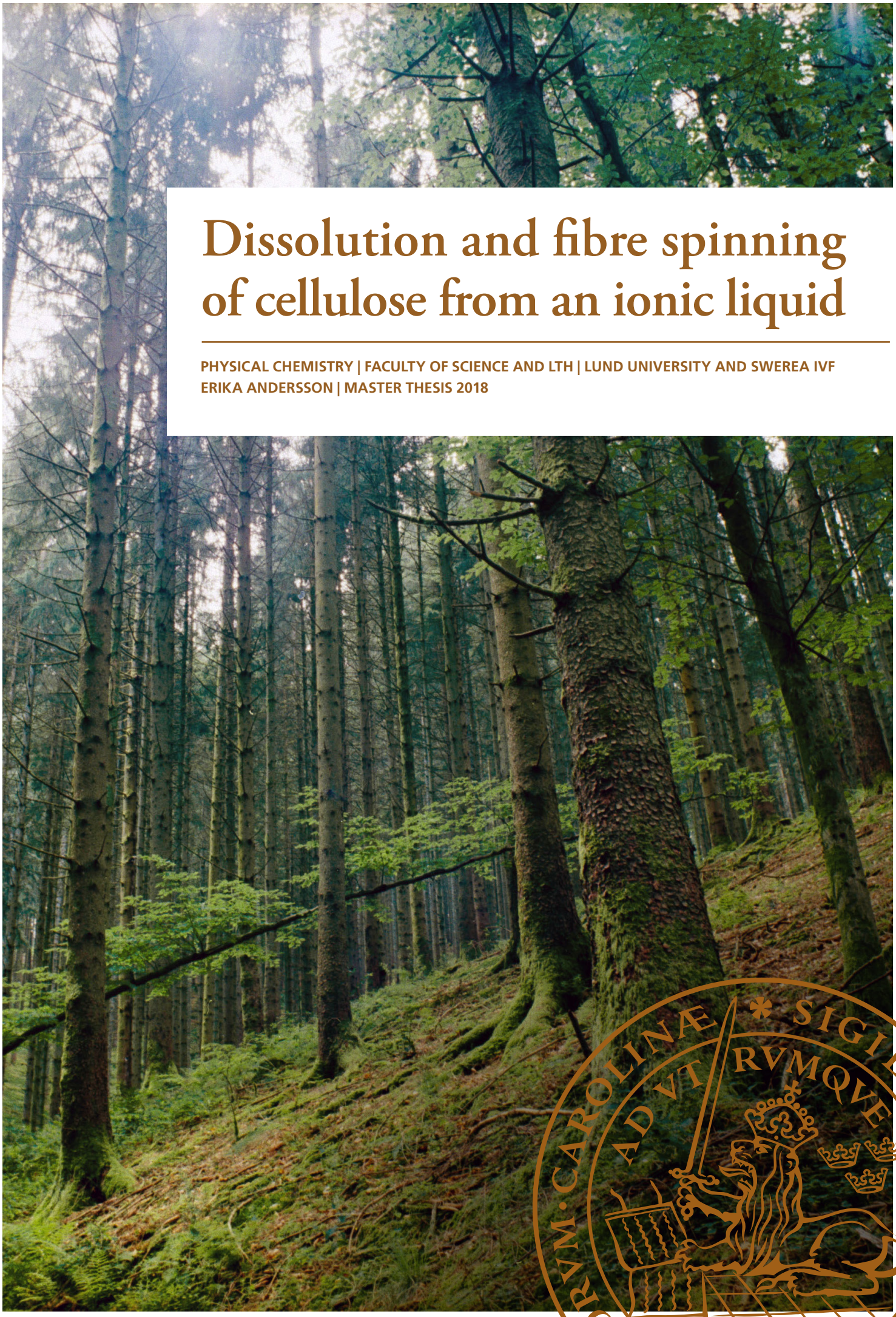

Dissolution and fibre spinning of cellulose from an ionic liquid

PHYSICAL CHEMISTRY | FACULTY OF SCIENCE AND LTH | LUND UNIVERSITY AND SWEREA IVF
ERIKA ANDERSSON | MASTER THESIS 2018

Dissolution and fibre spinning of cellulose from an ionic liquid

Master Thesis

Erika Andersson

Master of Science in Engineering, Engineering Nanoscience
LTH

Supervisor
Professor Ulf Olsson

Division of Physical Chemistry, Lund University

Assistant Supervisor
Tobias Köhnke

Division of Bio-based Fibres, Swerea IVF

Examiner
Professor Olle Söderman

Division of Physical Chemistry, Lund University

LUNDS UNIVERSITET
Lunds Tekniska Högskola

Abstract

Regenerated cellulose fibres can become a sustainable alternative to cotton and polyester in textile applications. One method of producing such is dissolution of cellulose in an ionic liquid (IL) and regeneration through air-gap spinning. In this master thesis, the dissolution state of cellulose in the ionic liquid 1-ethyl-3-methylimidazolium acetate (EmimAc) together with dimethyl sulfoxide (DMSO) has been studied through concentration series and diffusion nuclear magnetic resonance (NMR). It was shown that a stoichiometric relation of 3 or higher between the IL and anhydroglucose unit (AGU) is needed for complete dissolution and that one acetate ion bind to each AGU. In pure EmimAc, a structure of anions and cations is proposed to form around the polymer chain. The structure of the cellulose chains in solution was studied through small-angle x-ray scattering (SAXS) showing stiff cylinders with repulsive interactions. Rheological measurements were performed to evaluate spinnability of the solutions. Fibres were produced using air-gap spinning and the titer, tenacity, elongation at break and birefringence obtained at two different draw ratios (DR=4 and 6) and using two different coagulation mediums (water and isopropanol) were investigated. The level of crystallinity and internal fibre structure was evaluated using wide-angle x-ray scattering (WAXS) and SAXS. Fibres coagulated in water showed higher tenacity and a higher level of crystallinity but little dependence on the DR could be shown. An internal structure of 20 nm thick crystalline lamella in an amorphous matrix is proposed.

Popular Abstract

From tree to textile – cellulose dissolution and fibre spinning

I will make a guess: The clothes you are wearing are made of polyester or cotton, the two main textile fibres in use today. They are both related to several problems concerning sustainability but there are options on the way. This thesis investigates the dissolution of cellulose from wood and the spinning of textile fibres from this kind of liquid solution. It was shown to be a promising technique with many possibilities for future development.

The world's population is increasing and with it the need for a sustainable and renewable society. Textile and clothing is an essential part of our everyday life and which materials we use can have a large effect on our environment. Polyester is produced from oil and is therefore an unsustainable alternative. Cotton is a natural fibre but the production consumes huge amounts of water and land and harmful pesticides are often used. Also, we seem to have reached the limit of how much cotton that can be produced per year and there is a need to develop alternative fibres with similar properties.

One such alternative is regenerated cellulose fibres. Two types are already produced on industrial scale: viscose and lyocell, but more environmentally friendly production methods using less dangerous chemicals are needed. Cellulose is the most abundant biopolymer on earth, but it does not melt as most polymers do and therefore has to be dissolved to be processed. Special solvents are needed for this and in this thesis dissolution in the ionic liquid EmimAc is investigated. Ionic liquids are salts that are in liquid form at temperatures below 100°C. In solution the cellulose was shown to take the form of a stiff cylinder, only bending in segments of around 20 glucose units. This is thought to be because of a structure created around the chain consisting of alternating positive and negative ions coming from the EmimAc.

Fibres could successfully be spun from the cellulose/EmimAc solutions using a technique called air-gap spinning where the solution is extruded and stretched in an air-gap before being coagulated in a suitable medium. The coagulation medium is thought to affect the crystallinity of the fibre and thereby the mechanical properties. Here, fibres coagulated in water showed higher crystallinity than fibres coagulated in the alcohol isopropanol. Evaluation of the mechanical properties showed that the water fibres had potential of reaching strength comparable to viscose, lyocell and cotton. The main problem is that they have to be made thinner and still maintain these properties.

A structure which differs from what is commonly assumed for regenerated cellulose fibres was proposed. This constitutes crystalline lamella with a thickness of 20 nm ordered along the length of the fibre and surrounded by an amorphous matrix, as opposed to the common model which instead contains different amounts of needle-shaped micro-voids.

The main characterisation technique used in this work was x-ray scattering. It involves exposing a sample to a narrow x-ray beam that will be scattered by the particles in the sample and create a pattern on a detector. From this pattern, properties such as size, shape and interactions of the particles in the sample can be determined.

Preface

This master thesis was written as the final part of my education on Master of Engineering, Engineering Nanoscience with specialisation within materials science at LTH during the spring of 2018. The topic was chosen because of my interest in development of sustainable materials and the exciting possibility to try analysis techniques that will grow in importance in this region with the development of the Max IV synchrotron. The work was performed at the division of Physical Chemistry at Lund University in collaboration with the people at the division of Bio-based fibres at the research institute Swerea IVF in Mölndal.

I would like to thank my supervisor Ulf Olsson at the division of physical chemistry and assistant supervisor Tobias Köhnke at Swerea IVF for a very interesting project and good guidance along the way. I also wish to thank Jenny Bengtsson and Artur Hedlund at Swerea IVF for all the help with explaining and performing the fibre spinning and mechanical testing during my stay in Mölndal. Furthermore I want to thank Luigi Gentile for the help with the NMR and rheological measurements, Axel Rüter for guidance in various questions along the way as well as all the nice people at the division of Physical Chemistry for a memorable semester. A special thanks to all my friends and family who have supported me.

List of Abbreviations

Ac^-	Acetate ion
AGU	Anhydroglucose unit
BmimCl	1-butyl-3-methylimidazolium chloride
DMSO	Dimethyl sulfoxide
DP	Degree of polymerisation
EmimAc	1-Ethyl-3-methylimidazolium acetate
FID	Free induction decay
IL	Ionic liquid
IPA	Isopropanol
MCC	Micro Crystalline Cellulose
NaOH	Sodium hydroxide
NMMO	N-methylmorpholine-N-oxide
NMR	Nuclear Magnetic Resonance
SAXS	Small-angle x-ray scattering
SLD	Scattering length density
TBAAc	Tetrabutylammonium acetate
WAXS	Wide-angle x-ray scattering
wt%	Weight percent

Table of Contents

Cover picture by Martin Aurell, Forest in Schwarzwald, Germany

Introduction

The two main fibres used in clothing and textiles today are polyester and cotton and both have large environmental impact (Kalliala and Nousiainen 1999). Polyester is an oil based synthetic fibre making it directly unrenewable and to decrease the usage of fossil resources, the production of polyester should stop expanding. Cotton is a natural and renewable fibre but the production consumes large amounts of water, 1 kg cotton requires 3000-7000 litres of water, and many different types of fertilisers and pesticides are used to increase the yield (ICAC and FAO 2015). Large areas of land are also required for the cultivation, around 2.3% of the world's arable land was used for cotton production in 2013 (ICAC and FAO 2015). Considering the cotton production over the last years, it seems that the limit of how much cotton that can be produced per year using a comparable area of land is reached (The Fibre Year 2017). Considering a growing population, expected to reach 8.5 billion people in 2030 (UN 2017), which is in need of both clothing and land to grow food, cotton will not be able to act as single resource of renewable fibres and other types of fibres with similar properties as cotton are needed. In 2016, synthetic fibres accounted for 64% and natural fibres for 30% of the world fibre market. The remaining 6% constituted cellulosic fibres (The Fibre Year 2017).

Regenerated cellulose is one alternative source for renewable fibres that has gained much attention in recent years and that can be produced from for example wood pulp. Cellulose, being the most abundant biopolymer on earth has been used by mankind for millennia for everything from house building, clothing and paper as well as a source of energy (Klemm et al. 2005). It is a renewable source of raw material that exists almost everywhere on the planet in comparison to cotton that requires a very specific climate for large scale cultivation. A drawback is that cellulose does not exist in its pure form in nature but is linked with for example lignin and hemicellulose as is the case in wood (Bengtsson 2016).

Background

Cellulose is a linear polymer composed of repeating anhydroglucose units (AGUs) each approximately 8.5 Å in size (Milo et al. 2010) and covalently bonded by an acetal bridge between the OH-groups of C1 and C4 (1,4-β-linkage of glucose) as seen in Figure 1. Every second AGU is rotated 180° to accommodate for preferred bond angles. There are three hydroxyl groups located on each AGU making the cellulose chains strongly both intermolecular and intramolecular hydrogen bonding (dotted lines in Figure 1). Cellulose is a semi-crystalline material and the hydrogen bonds create a supramolecular structure of crystalline lamella with amorphous regions in between. This structure gives cellulose its characteristic properties such as infusibility, stability against mechanical load and insolubility in water and most organic solvents (Fried 2009; Klemm et al. 2005). The crystal structure of native cellulose, called cellulose I, consists of a monoclinic unit cell with cellulose chains oriented in parallel that form crystallites of up to 20 nm in cross section. When regenerated, cellulose instead forms the more stable structure cellulose II, which consists of antiparallel chains (Klemm et al. 2005). The degree of polymerisation (DP) (number of AGUs in the cellulose chain) depend on the origin and treatment of the cellulose spanning from 800-10000 for natural fibres, 300-1700 for wood pulp and 250-500 for regenerated cellulose fibres (Klemm et al. 2005).

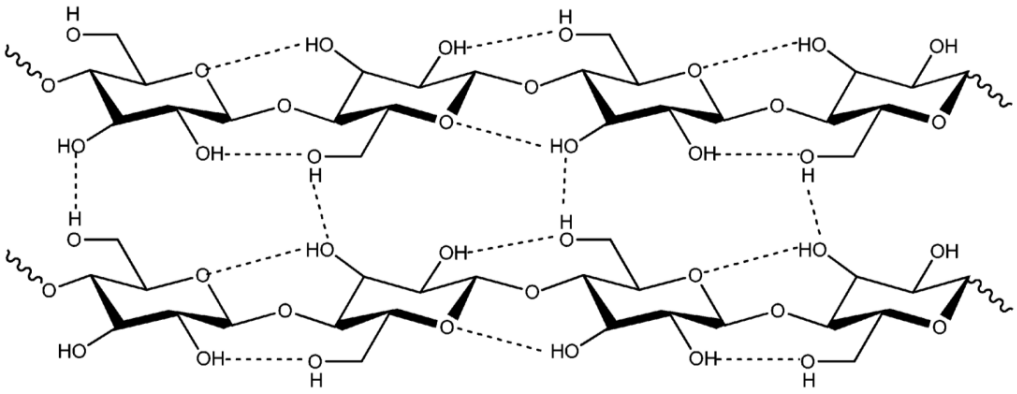

Figure 1. Molecular structure of cellulose, dotted lines represent intermolecular and intramolecular hydrogen bonds.

The main problem when processing cellulose compared to other polymers is the infusibility mentioned above i.e. cellulose does not melt at any temperatures before it breaks down. So to be able to create fibres, films, membranes etc. from cellulose, it must be dissolved before extruded into desirable shape and then regenerated (Gubitosi et al. 2016). An example of a process for doing this is air-gap spinning, used to create cellulose fibres that for example could be used in textiles. In this technique, the polymer solution is extruded through a round narrow opening, then passed through an air-gap where the flowing mass can be stretched to modify its properties and finally immersed into a medium in which the solvent but not the cellulose is soluble (Hedlund 2013). In this way, the cellulose is regenerated by coagulation during which it recrystallize. The main problem with this kind of processes is creating the polymer solution, because cellulose do not dissolve well in common solvents.

Four classes of cellulose solvents are currently known: phosphoric acid, NaOH-water, amine-oxides and ionic liquids (ILs) (Budtova and Navard 2016). All of them have their pros and cons but one group that has been intensively studied lately and showed good results for cellulose dissolution and regeneration is the ILs i.e. organic salts that are liquid at temperatures below 100°C due to a bulky cation that do not fit well into a crystal lattice (Hedlund et al. 2017; Isik et al. 2014). The ILs ability to dissolve cellulose is coupled to small hydrogen bond accepting anions that can compete with the hydrogen bonding between the cellulose chains. However, the cations can help to increase the solubility if having strong acidic protons (Isik et al. 2014). Some advantages of ILs are very low vapour pressure, nonflammability, high electrochemical and thermal stability and the possibility to tailor the properties by changing the chemical structure of cat- and anions (Budtova and Navard 2016). Some drawbacks with ILs are that they generally are expensive and have a high viscosity but this can be solved by diluting with aprotic polar solvents e.g. dimethyl sulfoxide (DMSO) (Hedlund et al. 2015).

Two types of textile fibres made from regenerated cellulose exist today in industrial scale: viscose and lyocell. Compared to cotton they consume 7-15 times less water per kilogram fibre and need ca 50% of the land area for cultivation (Bengtsson 2016). Viscose is produced through a derivate method which dates back to the early 1900s. It is a complex technique that requires high pureness of the cellulose used and include carbon disulphide (CS_2), sodium hydroxide (NaOH) and heavy metal compounds. To meet today's environmental standards, well developed techniques for optimisation of chemical use, purification of waste water and emissions are needed (Klemm et al. 2005). The alternative, which is often promoted as more environmentally friendly, is lyocell which is produced through a direct method developed in the 1980s based on dissolution at 80-120°C in N-methylmorpholine-N-oxide (NMMO) which can be almost completely recovered from the coagulation bath. This process also does not require as high pureness of cellulose but NMMO is a strong oxidising agent and has limited thermal stability making the use of it in industrial scale problematic (Klemm et al. 2005).

Dissolution and regeneration properties of different ionic liquids

In a study by Kosan et al. a comparison of cellulose solutions made using different ILs as well as NMMO is done together with an evaluation of the properties of fibres spun from these solutions (Kosan et al. 2008). They conclude that ILs with acetate (Ac^-) anions are more efficient in cellulose dissolution and can create solutions of higher cellulose concentrations compared to ILs with chloride anions, making acetate ILs more suitable for the shaping process of regenerated cellulose (Kosan et al. 2008). Acetate ILs also gave fibres with higher elongation values whereas chloride ILs gave higher tenacity. Using the cation 1-N-Butyl-3-methylimidazolium (Bmim) resulted in a higher viscosity compared to 1-ethyl-3-methylimidazolium (Emim) which can be a problem when dissolving and flowing the solution during spinning. Overall the ILs seemed to give fibres with comparable properties as NMMO (Kosan et al. 2008).

Similar findings as made by Kosan et al. are made in a study by Vinogradova and Chen comparing fibre spinning from 1-ethyl-3-methylimidazolium acetate (EmimAc) and 1-butyl-3-methylimidazolium chloride (BmimCl) (Vinogradova and Chen 2015). EmimAc is considered the better candidate for dissolving cellulose and spinning regenerated cellulose fibres for a number of reasons. Some of these are lower dissolution and spinning temperatures, more favourable tensile strength and crystallinity obtained for the fibres and better thermal stability of the IL. Another aspect is that the residuals of EmimAc that in some cases could be present in the finished fibre even after washing are non-toxic. This study also concluded that crystal size and crystallinity of the fibre can be increased by solution shearing during extrusion (Vinogradova and Chen 2015).

EmimAc is soluble in water while cellulose is not, so upon extrusion into a water bath the cellulose will coagulate and a fibre can be obtained. Since ILs are so expensive, being able to retrieve the solvent from the coagulation medium and reuse it is absolutely essential for industrial scale production. Water is a very pleasant substance to work with (affordable, abundant and does not bring risks on handling) but unfortunately EmimAc and other ILs have shown a limited long-term thermal stability at the temperatures needed to evaporate water and thereby retrieving the solvent. Therefore trials are made with coagulation in alcohols where lower temperatures can be used for solvent separation (Hedlund et al. 2015). The choice of coagulation medium likely affect the level of crystallinity in the spun fibre and material properties of cellulose depend on factors such as size, shape, orientation and concentration of the crystalline domains. Since the crystallinity thereby affect physical properties such as tensile strength, elongation at break and swelling which are important for textile fibres, it is important to understand the effect of the coagulant when developing a functional system for fibre spinning (Budtova and Navard 2016).

Exactly how Ac^- bind to cellulose during dissolution in ILs is not known. Dissolution of cellulose in the IL tetrabutylammonium acetate (TBAAc) together with DMSO has been shown to follow a solubility limit of one acetate per AGU that together with computer simulations propose that the ion bind to two OH-groups on the same AGU (Idström et al. 2017). However, similar studies for EmimAc in DMSO show different limits, from 1.5 Ac^- per AGU (Olsson et al. 2014) to 2.5-3 Ac^- per AGU (Le et al. 2014) proposing that one Ac^- bind to each OH-group. This raises questions of what affects the dissolution, more than the accessibility to Ac^-. The solubility limit and the mechanism behind it is important to understand when developing a system for fibre spinning and possible upscaling.

Scope of this thesis

With this as a background, the purpose of this master thesis is to look at possibilities to develop more sustainable alternatives of textile fibres, more specifically regenerated cellulose fibres from systems of cellulose and EmimAc. The solubility limit of cellulose in EmimAc/DMSO has been studied by visual

inspection of concentration series and the dissolution state by diffusion nuclear magnetic resonance (NMR) to evaluate the number of bound Ac^- per glucose unit under present conditions. Further analysis of the cellulose structure, both in solution and in spun fibres, has been done by rheology measurements, polarised optical microscopy, small-angle x-ray scattering (SAXS) and wide-angle x-ray scattering (WAXS). This was done to gain information about the polymer chains behaviour in the solvent and the crystal structure and ordering achieved in the fibre on spinning. Fibres coagulated in water or isopropanol (IPA) were compared. Spinning of fibres has been done using air-gap spinning and the mechanical properties were evaluated by tensile testing.

Materials and Methods

Materials

Two different substrates of cellulose were used. Micro crystalline cellulose (MCC) Avicel PH-101 with an approximate molecular weight of 29 kg·mol^{-1} (Gentile and Olsson 2016) was obtained from Sigma-Aldrich and dried at 80°C in an oven for at least two hours before use. Pulp in the form of sheets was provided by Södra and had a molecular weight of approximately 162 kg·mol^{-1} (Gentile and Olsson 2016). The sheets were cut into small pieces and dried in the same way as the MCC. For preparation of solution for fibre spinning the sheets were dried at 60°C and then chopped and ground at 1mm. The molecular weight of one AGU is 162.06 g·mol^{-1} and the density of cellulose is 1.5 g·cm^{-3}.

EmimAc with a purity of 97%, containing ≤0.5% water, obtained from Sigma-Aldrich was used as received. EmimAc with the same purity but containing ≤1.5% water obtained from Manchester Organics was melted in an oven at 50°C as it was received in solid state. EmimAc has a melting point of >30°C but can occur as an under cooled melt (Sigma-Aldrich). The molecular weight of EmimAc is 170.21 g·mol^{-1} and the density is 1.027 g·cm^{-3}(Sigma-Aldrich).

DMSO with a purity of ≥99.9% was obtained from Sigma-Aldrich and used as received. It has a molecular weight of 78.13 g·mol^{-1} and a density of 1.1 g·cm^{-3}(Sigma-Aldrich).

Isopropanol (IPA) with ≥98% purity was obtained from VWR Chemicals and used as received for coagulation of fibres.

Commercial fabric softener from the brand Neutral was used as received.

Methods

All plots were made using Matlab unless otherwise specified.

Dissolution

Stock solutions of 10, 20, 30 and 40 wt% EmimAc in DMSO were prepared and stored in glass bottles. The EmimAc concentration in weight percent was calculated as

$$c_{EmimAc} = \frac{100 \cdot m_{EmimAc}}{m_{EmimAc} + m_{DMSO}} \quad (1)$$

where *m* is the mass of the respective components. Similarly, cellulose concentrations in weight percent were calculated as

$$c_{cellulose} = \frac{100 \cdot m_{cellulose}}{m_{cellulose} + m_{EmimAc} + m_{DMSO}} \quad (2)$$

Samples containing between 3 and 15 wt% MCC were prepared by weighing the MCC in glass vials followed by the addition of the respective stock solution with a glass pipette. Samples were stirred with a magnetic stirrer in room temperature until dissolved or for a total time of three days. Visual inspection and cross polarised light was used to evaluate if the cellulose was molecularly dissolved. The solubility of MCC was plotted against the mass fraction of EmimAc to determine the solubility limit.

NMR

To investigate the number of cations, anions and DMSO molecules associated with each AGU in the cellulose, diffusion NMR was performed. In NMR the magnetic spin of the atomic nuclei is aligned with a strong external magnetic field, B_0, and then shifted to a certain angle using a radio frequency pulse which creates an overall magnetisation, *M*. When the nuclei relaxes back to alignment with B_0, the magnetisation disappears and the time this takes depends on the chemical environment of the nuclei

and is measured and called the free induction decay (FID). By Fourier transforming the FID signal, a spectra with peaks corresponding to each nuclei of specific chemical environment is obtained (Callaghan 1991). In this way nuclei (often ^{1}H or ^{13}C) present in the sample and their relative position within a molecule can be identified. The net displacement of whole molecules is also accessible with NMR and based on measurements of diffusion. As first described by Stejskal-Tanner in 1965 the diffusion coefficient *D* can be obtained from the echo amplitude *I*, measured in NMR pulsed spin echo experiments as

$$I = I_0 e^{-bD} \tag{3}$$

where

$$b = (\gamma \delta G)^2 \left(\Delta - \frac{\delta}{3}\right) \tag{4}$$

Here I_0 is the amplitude at G=0, γ is the gyromagnetic ratio, δ is the duration time of the radio frequency pulse, G is the strength of the pulse and Δ is the separation time between two pulses (Stejskal and Tanner 1965; Stilbs 1987). By plotting data as *I* vs *b* and fitting an exponentially decaying function, *D* can be obtained.

Samples with three different types of solvents where measured: 10 wt% EmimAc in DMSO and 1-3.5 wt% MCC, 20 wt% EmimAc in DMSO and 1-9 wt% MCC and pure EmimAc with 0.5-10 wt% MCC. Samples containing DMSO were prepared as described in the section on dissolution. For samples with pure EmimAc the solvent was first measured before addition of MCC in small portions with ultra-sonication (3000 min^{-1}) in between to avoid lumping. The samples were stirred with a magnetic stirrer and heated (temperature varied with viscosity but not over 80°C) to speed up the dissolution. Samples were transferred to 5 mm NMR glass tubes (Armar Chemicals, 5TA, 178 mm) using syringes and centrifuged if needed for the sample to enter the bottom.

^{1}H spectra were recorded to identify the origin of each peak using a Bruker Avance DMX200 spectrometer operating at 200 MHz with a 30° pulse, acquisition time of 400 ms, relaxation delay of 2 s and 8 scans. The peaks were identified and spectra were processed using the software MestReNova. The DMSO peak, if present, was used to calibrate the chemical shift.

Diffusion experiments were performed using pulsed gradient stimulated echo on ^{1}H nuclei using the same instrument. A commercial diffusion probe (DIF-25 5 mm) having a maximum gradient strength of 960 $G \cdot cm^{-1}$ was used. For samples with DMSO a gradient of 75 $G \cdot cm^{-1}$ was used and for samples with pure EmimAc a gradient of 284-390 $G \cdot cm^{-1}$. The gyromagnetic ratio used was 4.3 $kHz \cdot G^{-1}$, the duration of the field gradient pulses were 2 ms and the separation 140 ms for samples with DMSO and 100 ms for samples with pure EmimAc. The measurements were performed at 25°C using the instruments temperature control based on dry air. The software Topspin 2.0 (Bruker) was used to calculate the diffusion coefficients using peak integration and fitting of the exponentially decaying data based on area. Diffusion coefficients were plotted for each solvent species as a function of MCC concentration and the number of bound species per AGU calculated.

SAXS – solutions

SAXS measurements were performed on solutions of EmimAc and MCC or pulp respectively to determine the structure of the polymer chains in solution and possible interactions between them. DMSO was not included in this study because of strong x-ray absorption by the sulphur. SAXS is a scattering technique suitable for soft matter that can resolve structures in the size range of 0.5-500 nm. When exposing a sample to an x-ray beam, some of the incoming photons will interact elastically with the electron clouds of the atoms in the sample and be scattered. This creates a two dimensional

scattering pattern with varying intensities *I* depending on angle from the incident beam. By azimuthal averaging of the intensities, a graph of *I* vs *q* can be obtained where *q* is the momentum transfer between the incident and the scattered beam and is called the scattering vector. It is defined as

$$q = \frac{4\pi}{\lambda}\sin\frac{\theta}{2} \quad (5)$$

where λ is the wavelength of the incoming x-rays and θ is the scattering angle relative to the incident beam. The recorded intensity depends on the number of particles *N* in the scattering volume exposed by the beam, the difference $\Delta\rho$ in scattering length density (SLD) between particles and solvent, the particle volume V_p, a form factor *P(q)* describing the shape of the individual particles and a structure factor *S(q)* describing their interactions:

$$I = N\Delta\rho^2 V_p^2 P(q)S(q) \quad (6)$$

Particles scatter differently depending on their material. X-rays are scattered due to interactions with electrons and the SLD therefore depends on the electron density of the material. We calculate it as

$$\rho = \frac{\sum_i^n b_i}{\bar{V}} \quad (7)$$

where b_i is the scattering length of atom *i* and *V* is the molecular volume containing *n* atoms (Jackson 2013). A sufficient difference in SLD is needed between the sample and the solvent to get contrast and a good scattering signal.

In a dilute system, particle interactions can be neglected and S(q)=1. The shape of the graph of I vs q then represents the form factor which contains information about the size and shape of the particles in the system. Following the graph from small q-values towards larger can be compared to looking at the whole particle and then zooming in. Figure 2 a) show an example of a scattering curve obtained for a polymer in solution such as schematically depicted in Figure 2 b). At small *q*-values the scattering intensity levels off, the so called the Guinier regime. The value of *q* where the slope change can be used to determine the radius of gyration, R_g, of the polymer. A slope of $q^{-5/3}$ is characteristic for a polymer coil (self-avoiding walk) and a slope of q^{-1} indicate one dimensional objects (a polymer coil can be seen as built up of many articulated cylinders). The *q*-value at the transition between these two slopes tell us the persistence length l_p which is the length of one stiff segment of the polymer coil before it bends. A slope of q^{-2} would have indicated a two dimensional object such as a lamellar structure. At high q-values the slope is q^{-4} marking the beginning of the Porod region. The transition to the Porod region show the smallest length in the particle, in this case the radius *r* of the polymer coil. Sometimes oscillations of the curve are visible in the Porod regime and the position of the so called characteristic minima, where destructive interference causes the scattered light to cancel out, can be used to determine the size of the particles. Smaller particles will give a first minima at a higher *q*-value (Lindner and Zemb 2002).

By extrapolating the intensity of dilute systems to *q*=0, where *P(q)* and *S(q)* are both unity, it is possible to extract the molecular weight of the scattering particles (Schnablegger and Singh 2011). When the system is no longer dilute, the structure factor start to affect the look of the graph *I* vs *q*. The structure factor contains information about interactions between particles in the system. A downwards bending of the scattering curve at low *q*-values indicate repulsive interactions and an upwards bending indicate attractive interactions between the particles (Pusey 2002; Schnablegger and Singh 2011).

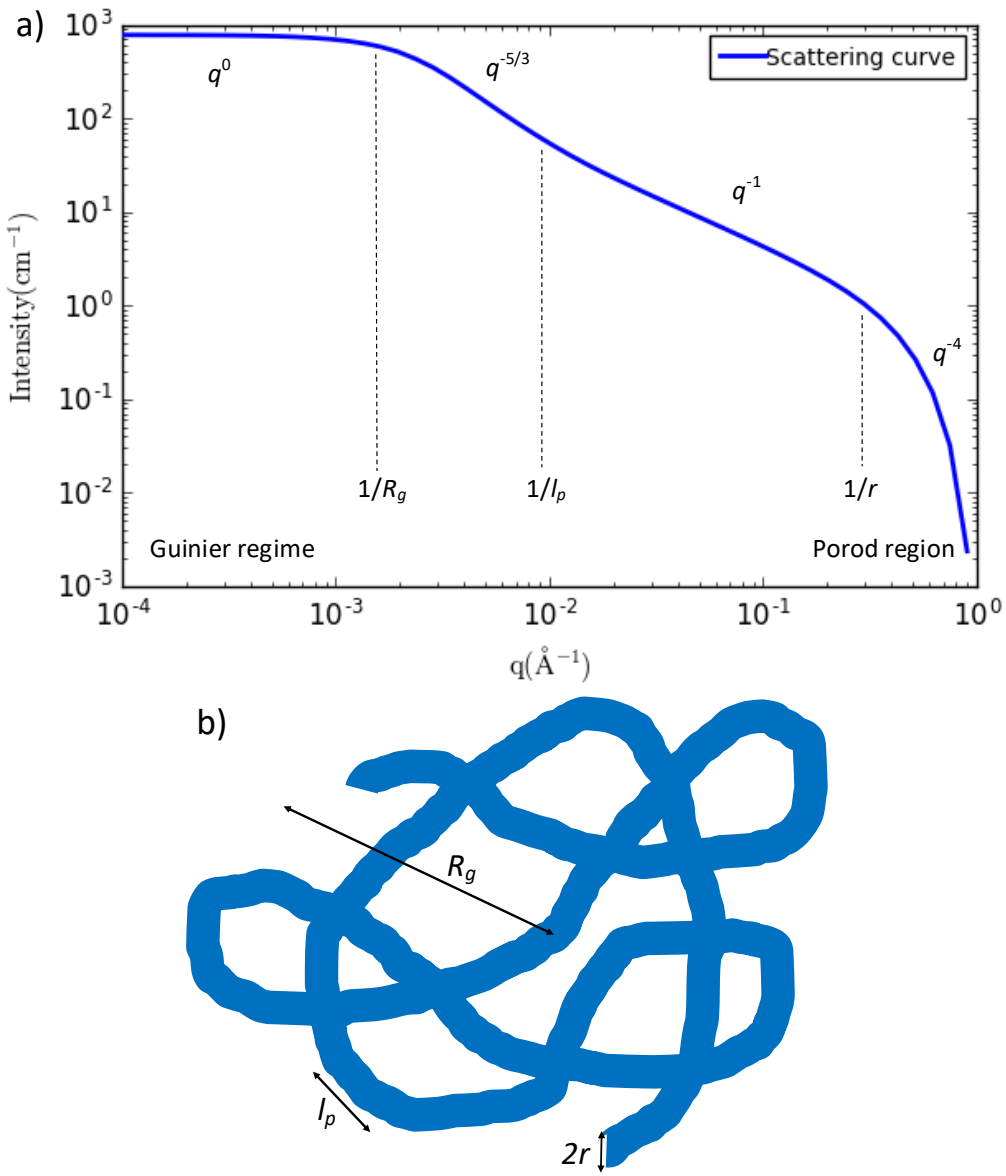

Figure 2. a) Graph of I vs q for the theoretical scattering from a polymer coil in a dilute system. b) Schematic illustration of a polymer coil

To be able to compare scattering intensity measurements performed at different instruments the data is transferred to absolute scale using a scaling factor. This factor is acquired by measuring scattering from water and comparing to a theoretical scattering value.

Samples of 0.5-15 wt% MCC and 0.5-10 wt% pulp respectively were prepared as described in the NMR section for samples of pure EmimAc. Samples were injected using syringes into 1.5 mm quartz capillaries (Hilgenberg, wall thickness 0.01 mm) mounted in metal holders. High viscosity samples were heated to make injection possible. Measurements were performed on a laboratory-based GANESHA instrument (SAXSLAB A/S) with a two-dimensional 300k Pilatus detector and a Genix 3D x-ray source with an x-ray wavelength of 1.54 Å. A two-pinhole set-up with a 2 mm beam-stop and two different detector distances giving a q-range of 0.005-0.7 Å^{-1} was used. The data was brought to absolute scale using the scaling factor of the instrument. Measurements were performed for 2-4 hours in vacuum at 22°C, controlled by an external water bath. The SLD of the solvent was calculated to $9.45 \cdot 10^{-6}$ Å^{-2} and the SLD of the cellulose to $1.36 \cdot 10^{-5}$ Å^{-2} using the software SasView. Data was processed and plotted as *I* vs *q* and theoretical fits were simulated in both Matlab and SasView.

Rheology

Rheology is used to characterise the dynamic behaviour of materials by measuring response to strain, induced by rotating or oscillating mechanical deformation. The strain span over which a material does not deform is called the linear viscoelastic region. Different types of materials have different stress response to the rate of strain i.e. shear rate and viscoelastic materials show a strong dependence of the shear rate. Homogeneous solutions of unbranched polymers (such as cellulose) can be described by a Maxwell element: a spring and a dashpot connected in series.

The elastic part of a Maxwell element is characterised by the storage modulus *G'* which is the component of the stress that is in phase with an oscillating strain. The viscose part is characterised by the loss modulus *G''* which is the component out-of-phase with the oscillating strain by 90°. The characteristics of a material is determined by measuring *G'* and *G''* as a function of angular frequency ω. At deformation rates slower than the relaxation time τ, such that the molecules can align with the shear direction, a material shows a viscose behaviour and *G''* dominates over *G'*. At fast deformation rates when the material does not have time to relax, *G'* dominates over *G''* and the material show a predominant elastic behaviour. The frequency at which the elasticity becomes more dominant than the viscosity is called the cross-over point (Mezger 2014). The quantity complex viscosity

$$\eta^* = \frac{G^*}{i\omega} \tag{8}$$

where

$$G^* = G' + iG'' \tag{9}$$

can be used to generate shear rate profiles from oscillatory frequency sweeps.

Rheological measurements were mainly performed to determine functioning concentrations and temperatures to use in air-gap spinning of solutions of cellulose and EmimAc. Previous testing at Swerea IVF had shown that a broad molecular weight distribution was desirable to obtain stable spinning when using EmimAc, together with a cross-over point at an angular frequency of 0.5-1 Hz and a complex viscosity of around 1000 Pa·s.

Samples of 1-15 wt% cellulose, in a 50/50 ratio mixture by weight of MCC and pulp, were dissolved in EmimAc as described for pure EmimAc in the NMR section. Dynamic strain sweeps were performed on an Anton Paar Physica MCR 301 rheometer equipped with a 1° truncated cone-plate geometry with a diameter of 50 mm to determine the linear viscoelastic region. Dynamic frequency sweeps at 0.1% strain were performed using the same instrument in the angular velocity range 0.01-100 s^{-1}. Measurements were made at 25°C controlled by a Peltier temperature control and for 10 wt% samples measurements were also made at 45°C and 60°C. Graphs of *G'* and *G''* as a function of angular frequency and complex viscosity as a function of angular frequency were made in OriginPro.

Dynamic frequency sweep was also performed at Swerea IVF in a temperature range of 25-60°C on the solution of 15 wt% cellulose prepared for spinning as described in the section Fibre spinning. A NOVA rheometer from REOLOGICA AB equipped with a plate-plate geometry with a diameter of 20 mm and a 0.5 mm gap was used. The angular velocity range was 0.01-50 s^{-1} and the strain was 0.01%. Graphs were made in Excel.

Fibre spinning

Fibres were spun using air-gap spinning as mentioned in the introduction. This is a type of wet-spinning where the polymer solution is extruded through a spinneret, passed through a small air-gap and then passed through a bath of non-solvent to coagulate the polymer as seen in Figure 3.

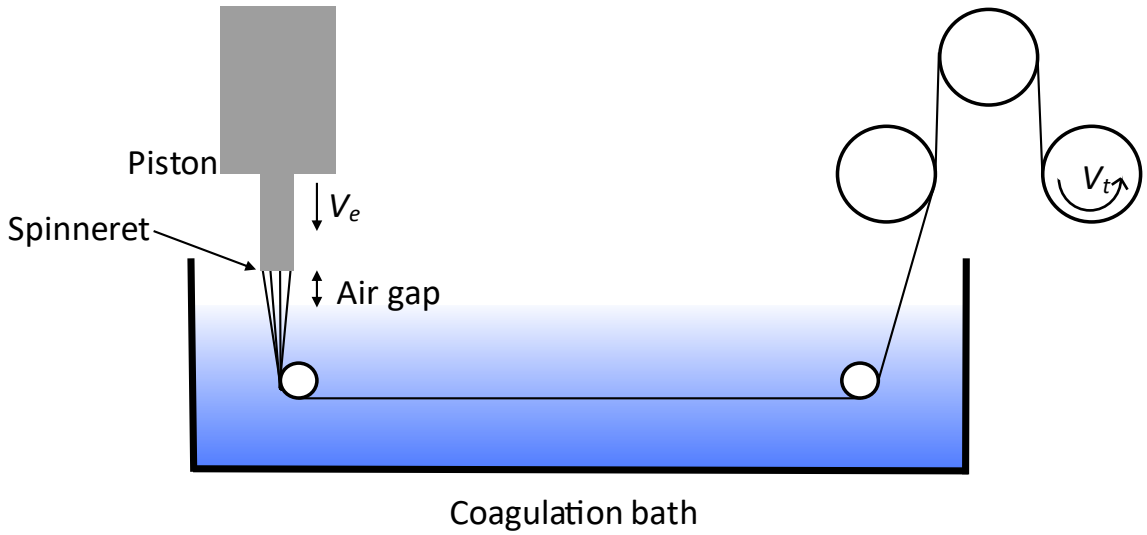

Figure 3. Spinning set up.

A difference in extrusion rate, V_e, of the solution and take up rate, V_t, of the fibre will result in a stretching defined by the drawing ratio as

$$DR = \frac{V_t}{V_e} \tag{10}$$

Stretching results in alignment of the polymer chains and crystallites along the fibre axis and also promote crystallisation which is shown to give a higher tensile strength and Young's modulus up to a DR of around 5 after which it levels off. A higher elastic modulus of the fibres may also be achieved by using a cold coagulation bath as the relaxation of the fibre alignment is lowered (Sixta et al. 2015).

15 wt% cellulose, in a 50/50 ratio mixture by dry weight of MCC and pulp, was dissolved in EmimAc by overhead stirring in a closed container heated to 80°C by an oil bath for 2 hours. The solution was transferred to spinning cylinders and deaerated at <100 mbar and 60°C over night to remove air bubbles that could cause rapture of the fibres during spinning. The homogeneity of the deaerated solution was confirmed between crossed polarisers using a Nikon Eclipse Ci POL light microscope. Fibres were spun using a customised laboratory spinning set up with a piston spinning unit shown in Figure 3. The solution was preheated for 45 minutes and extruded at 50°C with a 1 cm air-gap. A metal filter fleece with absolute fineness of 5 µm was inserted to remove possible undissolved particles before extrusion through a multi-hole spinneret with 33 holes of diameter 120 µm. The extrusion rate was fixed to 4 m·min^{-1} and the take up rate to 16 m·min^{-1} and 24 m·min^{-1} giving a DR of 4 and 6 respectively. Fibres were coagulated in a 1.5 litre bath of deionised water or IPA at 2-10°C and washed in deionised water or IPA overnight. Finally the fibres were washed in deionised water or IPA with 1% fabric softener for 1 hour and dried isometric (on rolls) at 80°C for 45 minutes. Table 1 summarise the three different preparation paths for fibres and the resulting six different types of fibres.

Table 1. Preparation paths for spun fibres.

Draw Ratio	Coagulation bath	Washing	Washing + softener
4	H_2O	H_2O	H_2O
4	IPA	H_2O	H_2O
4	IPA	IPA	IPA
6	H_2O	H_2O	H_2O
6	IPA	H_2O	H_2O
6	IPA	IPA	IPA

Mechanical properties

Linear density, conditioned tenacity and elongation at break was measured to evaluate the mechanical performance of the fibres. Linear density is measured in the unit tex where 1 tex=1 g·1000 m^{-1} (or 1 dtex=1 g·10000 m^{-1}) and used as a parameter when characterising textile fibres referred to as titer. Titer can be measured gravimetrically or using a vibroscope where the resonance frequency is determined. Commercial fibres have a titer of 1-2 dtex (Sixta et al. 2015). Tenacity is the measure of specific strength of fibres and yarns. It is the load at breaking divided by the linear density of the fibre and has the unit of $N \cdot tex^{-1}$ (or more applicable $cN \cdot tex^{-1}$). The tenacity is thought to increase with alignment of chains parallel to the fibre axis (Asaadi et al. 2018). Elongation at break is measured as percentage of the initial length. In regenerated cellulose fibres the elongation is thought to originate partly from ordering of the crystalline regions but also together with straightening of chains in the amorphous regions. Strength properties of regenerated cellulose fibres are in general weakened by moisture due to breakage of hydrogen bonds in the accessible amorphous regions (Sixta et al. 2015). Table 2 summarises the tenacity and elongation of some commercial fibres in conditioned state.

Table 2. Tenacity and elongation at break of some commercial fibre types (Bengtsson 2016; Hu and Hsieh 1997; Rieter).

Fibre	**Cotton**	**Polyester**	**Viscose**	**Lyocell**
Tenacity [cN/tex]	15-40	50-71	23-30	39-50
Elongation [%]	6-10	50-70	15-30	10-15

Linear density was measured using a Vibroskop 400, Lenzing instruments, with 300 mg pretension. Conditioned tenacity and elongation was measured using a Vibrodyn 400, Lenzing instruments, operating at a gap length of 20 mm and a stretching velocity of 20 $mm \cdot min^{-1}$. Ten samples of each fibre type were tested at 21°C and 65% relative humidity.

Polarised light microscopy

Birefringence measurements using polarised light microscopy were performed to determine the average orientation of the fibres. Fibres are anisotropic materials with different refractive index along the fibre direction, n_f, compared to across the fibre, n_t, making light that pass through the fibre change its polarisation. This can be measured as

$$\Delta n = n_f - n_t = \frac{R}{t} \qquad (11)$$

where R is the retardation of the light passing through the fibre and t is the thickness of the fibre. A higher value of Δn indicates more oriented fibres and the maximum value for cellulose fibres, indicating perfect orientation along the fibre direction, is often considered to be 0.062 (Sixta et al. 2015). The retardation can be measured using a uniaxial crystal called Berek compensator together with two polarisers at 90° angle respective to each other. The Berek compensator is tilted until maximum darkness is achieved in the fibre as seen in Figure 4 b) and the tilt in degrees is read.

Birefringence was measured on 10 samples of each fibre type at 45° angle to the polarized light using a Nikon Eclipse Ci POL polarized light microscope equipped with a 3λ Berek compensator. The thickness of the fibres was calculated from the linear density in dtex (measured as described above) by assuming a circular cross section and using the cellulose density of 1.5 $g \cdot cm^{-3}$.

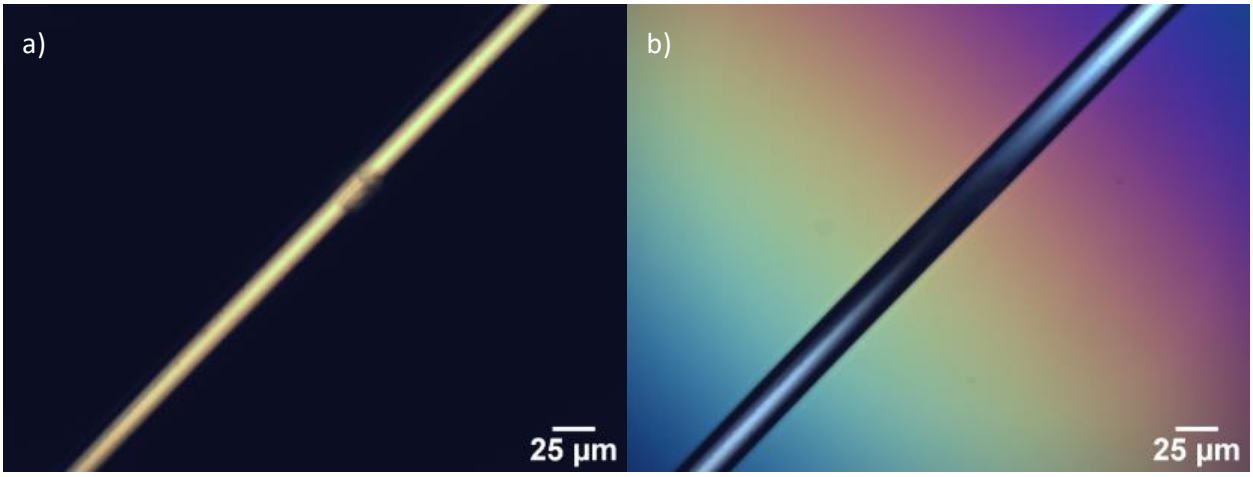

Figure 4. Determination of birefringence. a) One fibre in 45° angle to the polarised light, b) Berek compensator tilted until maximum darkness.

SAXS and WAXS – fibres

SAXS and WAXS measurements were performed to determine the internal structure and ordering of the fibres and map out the effect of the different spinning paths. In WAXS, the sample to detector distance is smaller than in SAXS making it possible to collect x-rays scattered at higher angles and thereby gaining information about smaller length scales, down to subnanometer. Here crystal structures and crystal orientations can be obtained. When performing x-ray scattering on solid samples there is a big contrast between the sample and the background which often is vacuum, compared to the contrast between a sample and a solvent.

As mentioned in the introduction, the amount of crystalline material and the arrangement of the crystallites affect the material properties of the regenerated cellulose. Since the 1950s, the common interpretation is that the anisotropic SAXS pattern usually arising from regenerated cellulose fibres is due to needle shaped micro-voids parallel to the fibre axis created during the spinning process. SAXS patterns are often used to characterise the size, shape and amount of these voids (Jiang et al. 2012). By looking at the scattering along the equatorial and meridional axis of the SAXS pattern the inner structure parallel to the fibre axis and perpendicular to the fibre can be examined respectively. WAXS patterns are normally used to index reflections to determine the unit cell i.e. type of cellulose, examine the orientation of the crystallites and the amount of crystalline material.

WAXS and SAXS measurements were performed on the same instrument as described previously. Fibres were counted, aligned in bundles that were mounted in a holder using tape and placed perpendicular to the x-ray beam. Measurements were performed in vacuum with acquisition times of 600s for WAXS and 3600s for SAXS in a q-range of 0.003-2.75 $Å^{-1}$. Two dimensional scattering patterns for WAXS and SAXS and azimuthal integrations along the equatorial and meridional axis for SAXS, were obtained using the software Saxsgui v2.15.01.

Results and Discussion

Solutions

Dissolution

The limit of dissolution for cellulose in EmimAc has previously been determined to 25-27 wt% (Le et al. 2014; Lovell et al. 2010). It was not in the interest of this thesis to investigate this further but rather to clarify the stoichiometric relation between AGU and Ac^- in EmimAc because of the contradictive data for ILs mentioned in the introduction. It is thought that the acetate, which is a particularly strong hydrogen bonding acceptor, binds to the OH-groups on the glucose unit and thereby breaks the hydrogen bonding between the cellulose chains making the dissolution possible (Navard et al. 2012). DMSO is also a hydrogen acceptor but much weaker than the acetate and does not by itself dissolve cellulose. Instead it is used as a co-solvent. The main purpose of the DMSO is to dilute the EmimAc to decrease the time of dissolution by lowering the viscosity and also consume less of the expensive EmimAc. Some studies show that the dilution of EmimAc with DMSO promotes the dissolution by lowering the ion association in the EmimAc thereby producing more free anions (Le et al. 2014).

The solubility of MCC as a function of EmimAc concentration with error bars is seen in Figure 5. The data do not follow a straight line very well and it seems like a higher relative amount of EmimAc is needed to dissolve higher wt% of MCC as seen in the study by Olsson et al. (Olsson et al. 2014). Plotted in Figure 5 is also a line representing a solubility limit of $n_{IL}/n_{AGU}=3$. The data seems to agree with this ratio of 3 n_{IL}/n_{AGU} needed for dissolution as concluded by Le et al. (Le et al. 2014) mentioned in the introduction and is far away from the one Ac^- per AGU found for TBAAc/DMSO in the study by Idström et al. (Idström et al. 2017). It can therefore be concluded that it is not only the stoichiometric amount of Ac^- that governs the dissolution but both the cation and the co-solvent take part in the dissolution mechanism and can change the dissolution properties. Because of limited time, these experiments were not repeated using pulp but it would have been interesting to see if the same behaviour apply in EmimAc/DMSO independent of molecular weight.

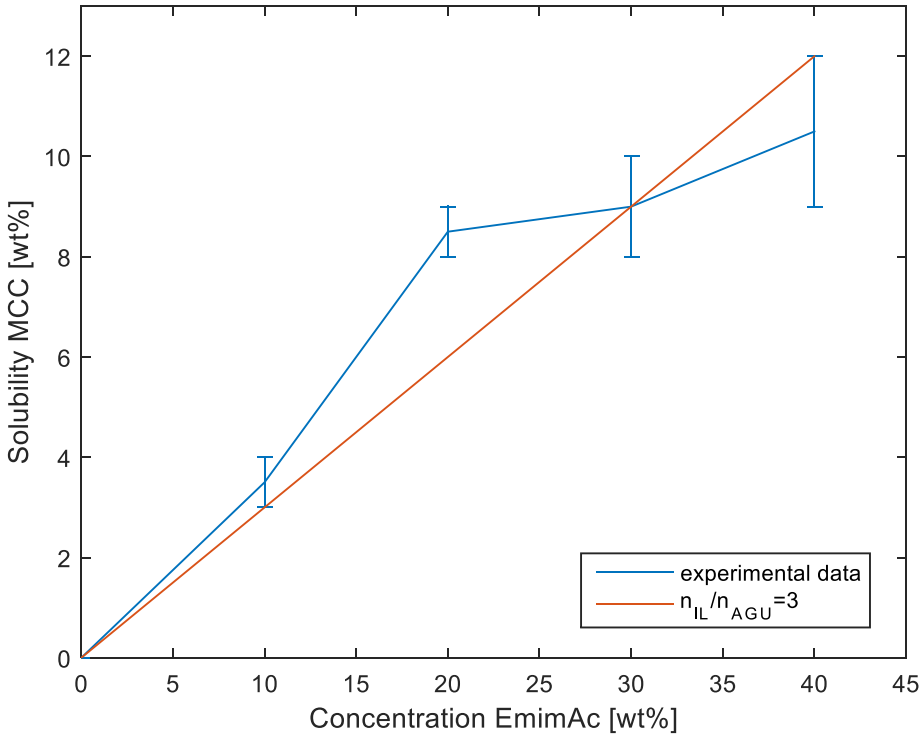

Figure 5. Solubility of MCC as a function of EmimAc concentration.

Impurities of water in the EimmAc used could affect the ratio determined since EimmAc is hygroscopic and water has been shown to lower the solubility of cellulose as it function as a hydrogen bond donor interacting with the acetate (Idström et al. 2017; Le et al. 2014). As the results agree with the ones presented by Le et al. (Le et al. 2014) it is not likely that the same amount of impurity occurred in both their study and this one. A graph with wt% MCC as a function of n_{IL}/n_{AGU} including all sample points can be seen in Appendix 1.

NMR

The molecular structures of EimmAc and DMSO are seen in Figure 6 a) and b) respectively and the corresponding ^{1}H spectres are seen in Figure 7 a) and b) with NMR peaks resulting from the respective labelled hydrogens in EimmAc identified in a).

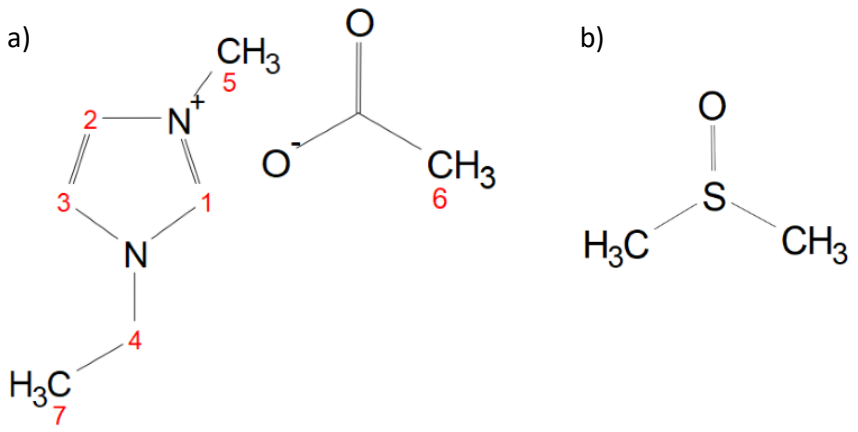

Figure 6. Molecular structure of a) EimmAc with hydrogens resulting in individual NMR peaks labelled and b) DMSO.

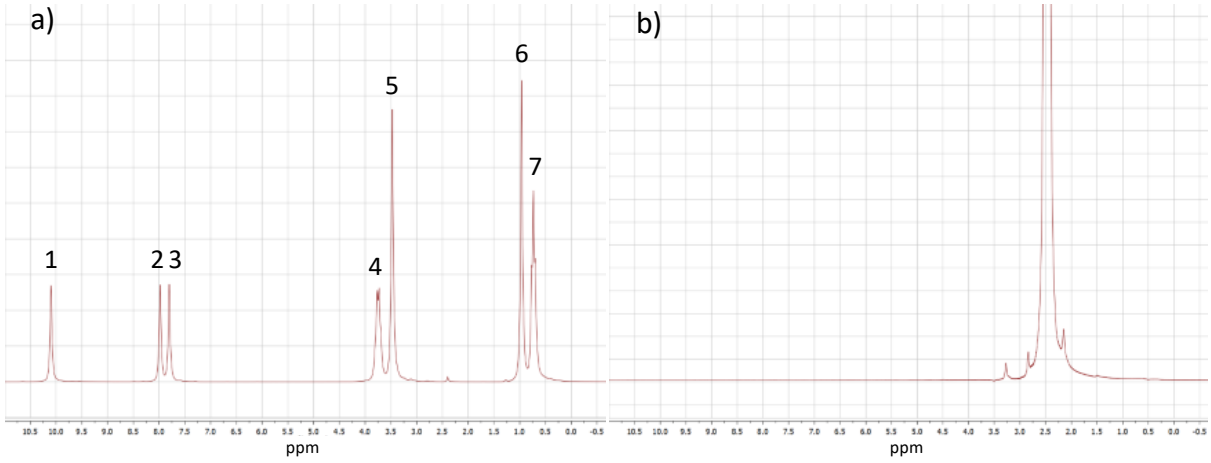

Figure 7. ^{1}H NMR spectra of a) EimmAc with individual peaks labelled and b) DMSO.

Peak integration was performed and diffusion coefficients *D* calculated for all the individual peaks. In the following evaluation, the cation diffusion is determined by the average of peaks 1-3, the anion diffusion from peak 6 and the DMSO diffusion from the DMSO-peak, see table of all values in Appendix 2. Peak 4 and 5 are excluded to avoid influence from the DMSO-peak and contaminating water which are close in ppm and peak 7 because of overlap with the anion peak. All integration values fitted well with a mono exponential decay which means the species only show one diffusion coefficient. This indicate that no aggregates or ion pairing are present in the sample alternatively fast exchange between such. In pure EimmAc the diffusivity was higher for the cation than the anion even though it is bigger. The anion diffusivity decreased slightly more with increasing cellulose concentration than the

diffusivity for the cation. For the 10 and 20 wt% EmimAc in DMSO the diffusivity was slightly higher for the anion than the cation but it still decreased more than the cation diffusivity as in the case of pure EmimAc. This could indicate that the DMSO facilitates the dissociation of the anion from the cation making it more accessible for dissolution. The larger decrease in diffusivity for the anion on increasing cellulose concentration suggests that it is more involved in the dissolution process and slowed down by binding with the polymer chain.

The observed diffusion of different solvent species in a solution with cellulose can be expressed as

$$D = (1 - P)D_0 + PD_c \approx (1 - P)D_0 \qquad (12)$$

where P is the fraction of species bound to cellulose, D_o is diffusion in pure solvent and D_c is the diffusion of cellulose in the solvent. The contribution from pure cellulose diffusion can be disregarded since diffusion of cellulose is very slow compared to the diffusion of solvent species. If a fixed number N of each species bind per AGU, equation 12 can be expressed as

$$P = 1 - \frac{D}{D_0} = N\frac{M_{species}}{M_{AGU}}\frac{c}{(1 - c)x} \qquad (13)$$

where $M_{species}$ is the molecular weight of the specific species, M_{AGU} is the molecular weight of one AGU, c is the mass fraction of cellulose in the sample and x is the mass fraction of the species in the solvent of the specific sample (Gentile and Olsson 2016). Figure 8 a-c) show plots of D/D_0 vs c/(1-c) for the three different solvent types tested (pure EmimAc and 10 and 20 wt% EmimAc in DMSO respectively). Linear regression to the data of the respective species in the solvent is used to determine N for Ac^- and DMSO (the hydrogen bonding species) after taking the different molecular weights (for Ac^- the molecular weight of the EmimAc is used) and solvent fractions into account, see Table 3. Figure 8 d-e) show N as a function of c for Ac^- and DMSO.

The diffusion of all species decrease with cellulose concentration indicating that they associate with the polymer chain. The calculated N in Table 3 is based on the assumption that a fixed number of each species binds to each AGU but as can be seen from Figure 8 a-c) the decrease in diffusion does not follow a linear relation. Instead one observes a decrease in N associated with cellulose upon increasing the concentration, Figure 8 d-f). The cation is not thought to bind to the AGU but associate with the already bound Ac^- and is therefore not evaluated.

From the graphs in Figure 8 b) and c), DMSO appears less influenced by the cellulose concentration since the slope is less steep. When accounting for the large weight fraction of DMSO in the samples, it shows instead to be highly associated with the polymer even if it is not the direct solvent (Figure 8 e) and f) and Table 3). The values of N are in fair agreement with what is found for TBAAc/DMSO by Idström et al. (Idström et al. 2017). There is no possibility for so many DMSO molecules to hydrogen bond to the AGU so the DMSO must have other types of bound states where it is also solvating the cellulose chain.

For the diluted solvents of 10 and 20 wt% EmimAc in DMSO, the number of bound Ac^- per AGU is close to 1.5 as concluded in the part about dissolution in the study by Olsson et al. (Olsson et al. 2014). This is in fair agreement to what is found by Idström et al. (Idström et al. 2017) where it was concluded that one Ac^- binds to two OH-groups on the AGU. In the case of that study the solubility limit also followed a ratio of one which is not the case in the dissolution study above where n_{IL}/n_{AGU} needed to be around three for complete dissolution to take place. This could partially be explained by the observation that a higher relative amount of EmimAc seems to be needed to dissolve higher concentrations of MCC. For samples of 10 and 20 wt% EmimAc the cellulose concentrations are relatively low and the relation of 3:1 is not yet reached (see Figure 4). As N increases slightly with increasing EmimAc concentration it

would have been interesting to see the results if NMR was performed also on the samples of 30 and 40 wt% EmimAc. Then the possible non-linear relationship could be further analysed and maybe it could be concluded how many Ac^- that actually bind to the OH-groups of the AGU. It is possible that only one Ac^- bind to the AGU but excess EmimAc is needed to create sufficient space between the chains for them to become molecularly dissolved and not associated with each other or that some Ac^- is lost to contaminating water.

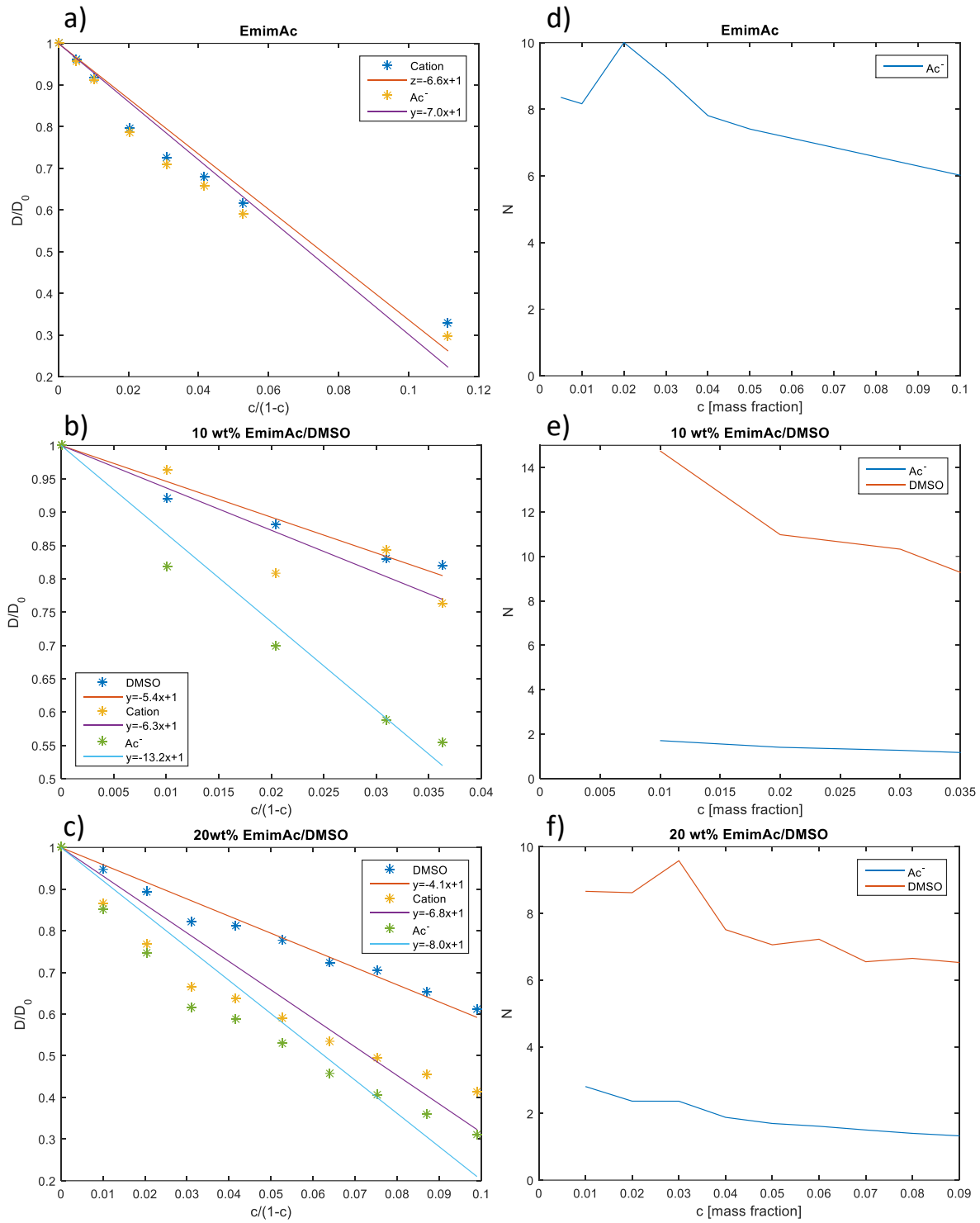

Figure 8. Plots of D/D_0 vs. c/(1-c) including linear regressions for DMSO, cation and anion in samples of a) pure EmimAc, b) 10 wt% EmimAc in DMSO and c) 20 wt% EmimAc in DMSO. Plots of N vs. c in samples of d) pure EmimAc, e) 10 wt% EmimAc in DMSO and f) 20 wt% EmimAc in DMSO.

Table 3. Calculated number of bound N of Ac^- and DMSO in the three different solvent types.

Sample	Species	$M_{species}/M_{AGU}$	x	Slope	N
EmimAc	Ac^-	1.05	1	7.0	6.66
10 wt% EmimAc	DMSO	0.48	0.9	5.4	10.13
10 wt% EmimAc	Ac^-	1.05	0.1	13.2	1.25
20 wt% EmimAc	DMSO	0.48	0.8	4.1	6.83
20 wt% EmimAc	Ac^-	1.05	0.2	8.0	1.52

The result of more than six bound Ac^- per AGU in pure EmimAc is surprising. Intuitively, there is not space for six anions to associate with each AGU and it would lead to a very sterically hindered polymer chain. Other aspects has to be taken into consideration when the solvent consists of only ions that are closely associated with each other without a co-solvent to help with dissociation and charge neutralisation. Probably the decrease in diffusion seen is not only due to direct binding to the cellulose chain but results from a structure created around the chain where alternating layers of anions and cations bind to each other. This would also explain why the cation mobility strictly follows the same pattern as the anion. It is possible that the anions associate in layers, where each layer is similar to its behaviour in DMSO. The dimensions or existence of these layers could be determined by WAXS analysis on the solutions.

A similar diffusion study by Ries et al. have found a number of *N*=3 agreeing with the idea that one Ac^- bind to each OH-group of the AGU (Ries et al. 2014). However in this study the reasoning is based on a population average of the activation energies of the free and bound state which is wrong when working with a dynamic parameter such as the diffusion constant.

SAXS

Graphs of *I* vs *q* on absolute scale and normalised with mass fraction for 0.5-15 wt% MCC is shown in Figure 9 a) and for 0.5-10 wt% pulp in Figure 9 b). Measurements down to q=0.005Å^{-1} were only done for concentrations of 0.5 wt%. When plotting the data of Figure 9 a) and b) together, the curves for corresponding concentrations of MCC/pulp overlap very well (figure left out because cluttered). The apparent difference in characteristic minima for the MCC samples, especially for 1 wt%, is an artefact due to over subtraction of background.

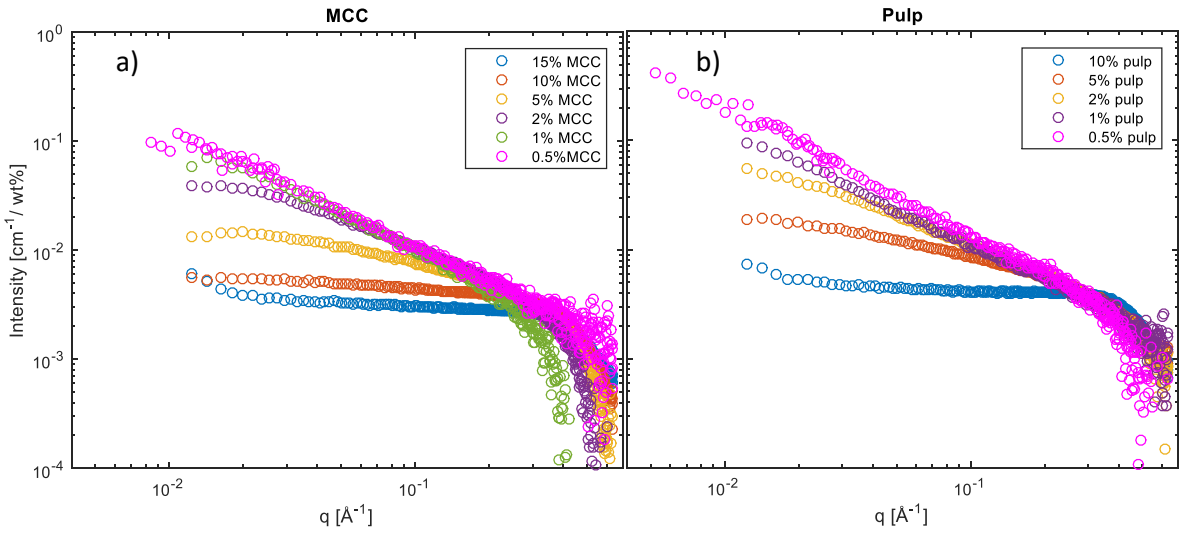

Figure 9. SAXS profile on absolute scale normalised with mass fraction for different concentrations of a) MCC and b) pulp in EmimAc.

A clear decrease in intensity at smaller q-values is seen for higher concentrations indicating repulsive interactions between the cellulose chains. A slope of q^{-1} is determined for the low concentrations, where there is no influence from a structure factor, proposing one dimensional objects (Lindner and Zemb 2002). This is interpreted as the cellulose chain arranging in the form of a cylinder on the length scale resolved.

The form factor for a flexible cylinder was used to fit the data from 0.5 wt% pulp using SasView, see Figure 10. This data was chosen as it covers the broadest q-range and shows no influence from a structure factor. The points at the highest q-values were considered as noise and removed before fitting to not mislead the software. The model describes a chain of total contour length *l* and radius *r,* consisting of locally stiff segments each with a length corresponding to the persistence length l_p (SasView 4.1.2 Documentation). The software was given the values for SLD of cellulose and solvent and rough adjustments were made before it was allowed to fit the radius *r* and the Kuhn length $l_k=2l_p$. The specific fit shown in Figure 11 is for a radius of 4.8 Å and a Kuhn length of 350 Å. Polydispersity was not considered in the fit. Since the data show a slope of q^{-1} over the entire *q*-range no information can be obtained about the total contour length of the cellulose chain but we know from the molecular weight that it is long in this context. What can be concluded from this analysis is that the cellulose chain in EmimAc behaves as a flexible cylinder with a radius of around 5 Å and a persistence length longer than the resolution limit (≈200 Å) of this experiment.

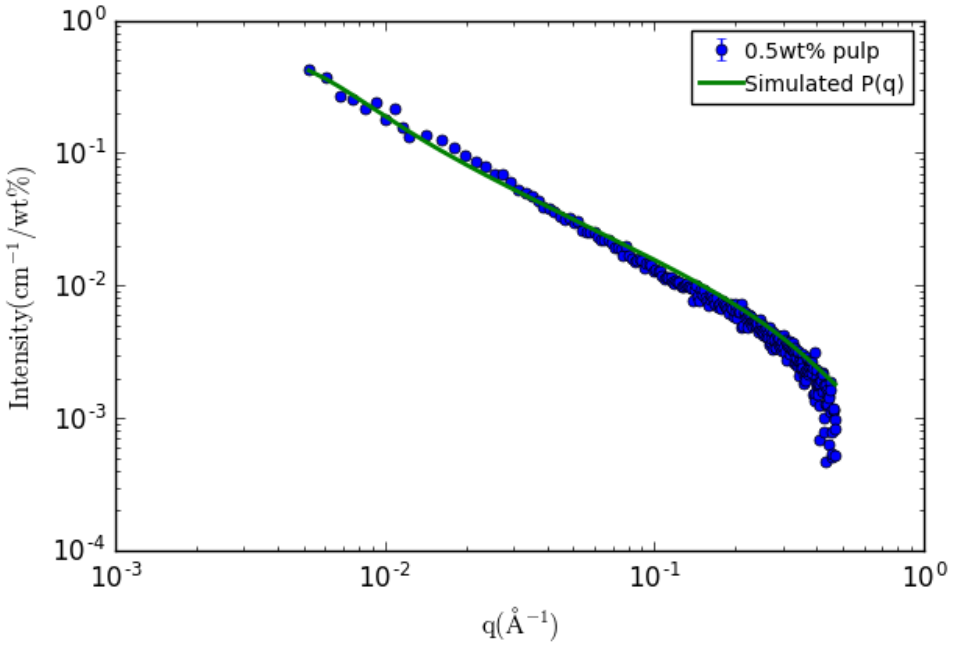

Figure 10. Data from 0.5 wt% pulp and simulated form factor for a flexible cylinder.

Experimental data from all the concentrations of pulp was fitted in Matlab using a model with a form factor for cylinders and including a structure factor

$$S(q) = \frac{1}{1 + \nu P(q)} \qquad (14)$$

where *ν*, the excluded volume, is 0 if no interactions are present in the sample and increases with increasing repulsive interactions i.e. increase with concentration. The Matlab script can be found in Appendix 3. Pulp was chosen as this data contains less noise and have a more accurate background subtraction. The correctness of the fit was determined visually and therefor data points at high *q*-values were not removed as for the SasView fitting. Since the data from pulp was shown to overlap

with that from MCC, these simulations are considered valid also for the samples with MCC. The parameters for radius and length were obtained from the best fit at the lowest concentration (0.5 wt%) with v=0 as this sample was considered unaffected by a structure factor. For higher concentrations only v is varied to obtain a fit as radius and length should not depend on concentration. The simulations are seen in Figure 11 a-e) and corresponds to a length of 10.000 Å, a radius of 4 Å and a v of 0 for 0.5 wt% ranging up to 1500 for the highest concentration (see respective values in the figures). Approximately equal fitting was observed for a total length of 15000 Å as again these length scales are far beyond the information obtained in this data.

In the Matlab simulations, the choice of simulated structure factor seems to agree fairly well with the data as agreement can be obtained by only varying v. However this structure factor is not applicable over a wide q-range and only applies to the semidilute region where binary contact between cellulose chains can be considered. The values obtained for the cylinder radius from Matlab and SasView agree and also agree with the literature values for the size of the glucose unite (Milo et al. 2010). There is no indication in the experimental SAXS data of reaching a plateau at low q-values (no Guinier regime visible) and therefore no exact value can be determined for the length of the cellulose chain, but it can be said that it is long relative to the persistence length.

The SAXS data show that the cellulose in solution behaves as a stiff chain which agrees with the picture from the NMR measurements, where six anions form a structure around each AGU making it sterically hindered. Unfortunately WAXS was not performed on these solutions so the presence of this kind of periodic structure cannot be concluded from the data. A Kuhn length of 350 Å (l_p=175 Å) as obtained from the SasView model would mean that the cellulose chain do not bend until after ca 20 AGUs. By just varying the parameters slightly it is possible to achieve equal fitting for Kuhn length of 200-500 Å. The persistence length for cellulose is known to vary with the solvent and the smallest recorded persistence length is 42 Å for tris(ethylenediamine)cadmium hydroxide (Cadoxen), while in LiCl/DMAc it has been estimated to 252 Å (Maeda and Inoue 2011).

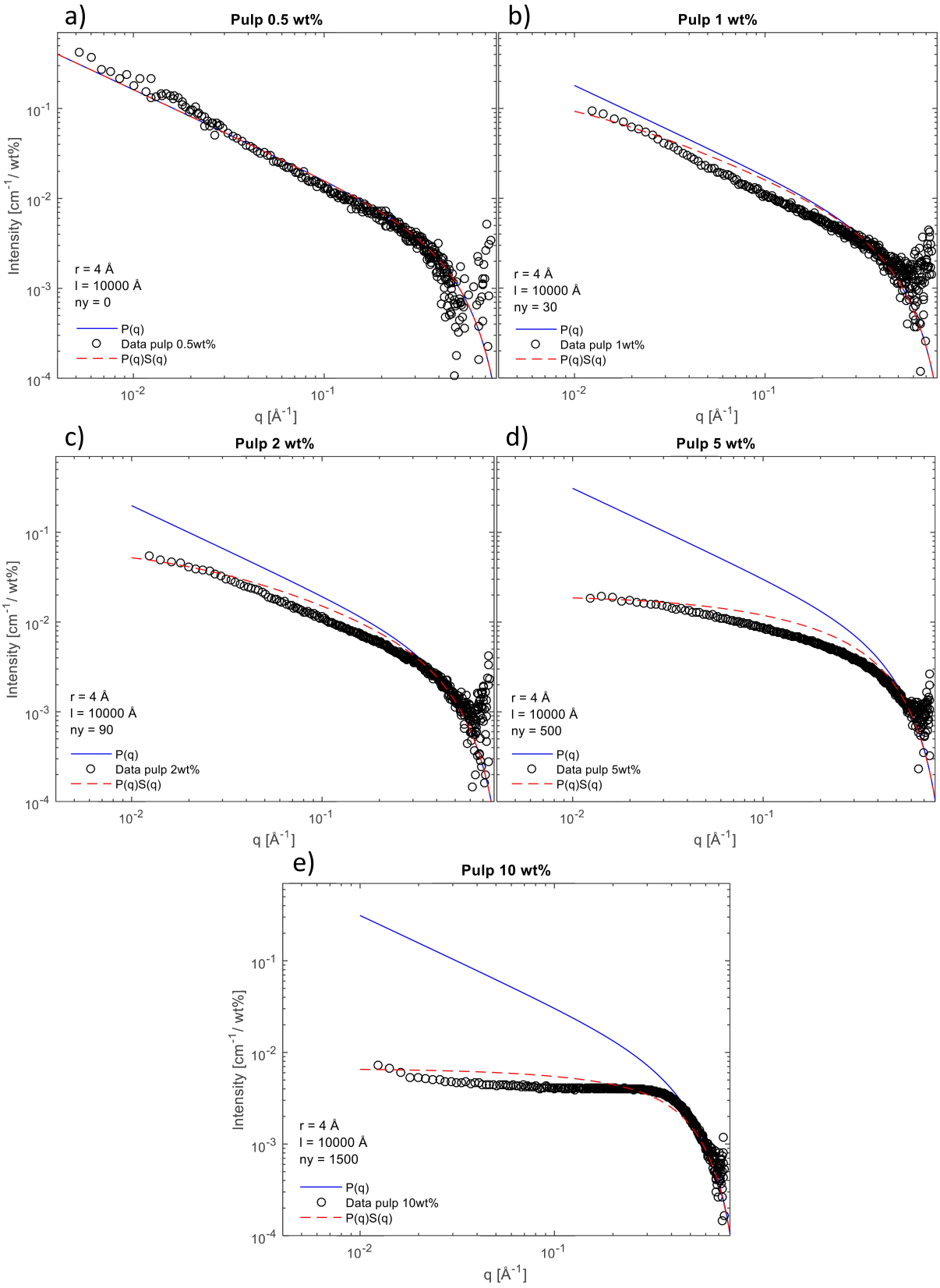

Figure 11. Simulated fits of form factor and structure factor to the experimental data of a) 0.5 wt%, b) 1 wt%, c) 2 wt%, d) 5 wt% and e) 10 wt% pulp in EmimAc.

Rheology

The spinnability parameters as stated by Swerea IVF, a complex viscosity of around 1000 Pa·s and a cross-over point at an angular frequency of 0.5-1 Hz, were sought. The complex viscosity for samples of 1-15 wt% cellulose at 25°C, Figure 12 a), show a promising appearance of spinnability for the 10 wt% sample. However, when also considering Figure 13 b), the samples of 1-10 wt% cellulose at 25°C had a cross over point above the spinnability window and for the 15 wt% sample it was below the measurable frequency. At higher temperatures, the cross over point for the 10 wt% sample moved to even higher frequencies and the complex viscosity decreased making it unsuitable for air-gap spinning whereby 15 wt% was chosen as cellulose concentration for the spinning trials. The complex viscosity and cross over point for 15 wt% cellulose at 45-60°C can be seen in Figure 13 a) and b). Based on this data a spinning temperature of 50°C was chosen.

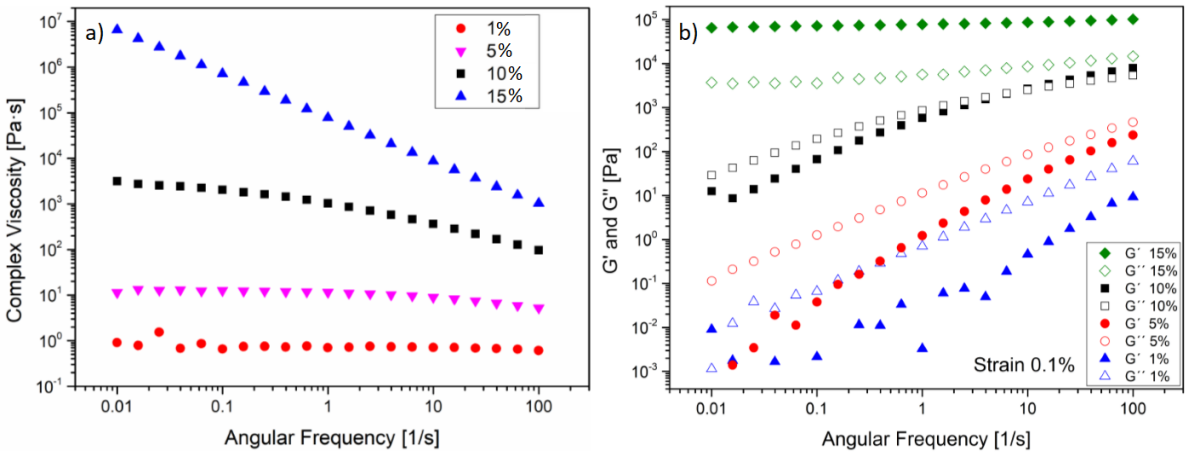

Figure 12. a) Complex viscosity and b) frequency sweeps indicating the shift of the cross over point with concentration for 1-15 wt% cellulose at 25°C.

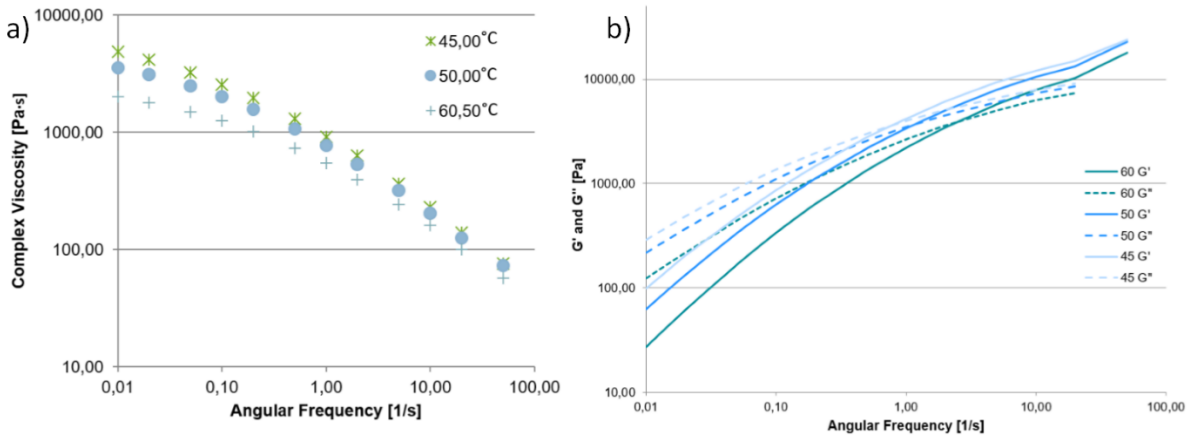

Figure 13. a) Complex viscosity and b) frequency sweeps indicating the shift of the cross over point with concentration for 15 wt% cellulose at 45-60°C.

What parameters are needed for good spinnability and why still needs to be evaluated further. One study has concluded good spinnability at an angular frequency of 1 s^{-1} or slightly over for the cross over point and a complex viscosity around 25000 Pa·s (Sixta et al. 2015). This is much higher than what was used here and previously concluded at Swerea IVF but adequate spinning seems to be achieved in both cases. The rheological parameters needed for good spinnability are likely to be highly dependent on the equipment and set up used.

Different solvents have different viscosities and therefore require different spinning temperatures to achieve good conditions. Preferably spinning is done at room temperature when considering industrial scale use to save time and energy. It is also important that spinning can be performed at a temperature far below the limit of thermal stability of the solvent. In the study mentioned above, good spinnability was found for NMMO at 95-100°C and at 70-75°C for the IL used (Sixta et al. 2015). A spinning temperature of 50°C as used here appears to be lower than what is used in most cases.

Fibres

Spinning

Microscopy pictures of the spinning solution after deaerating overnight did not show any undissolved particles which was confirmed by the lack of accumulating pressure in the extrusion cylinder during spinning, indicating a fully dissolved and homogenous solution. The maximum DR without fibre breakage was 7.5 when using water as coagulant and 6 when using IPA. Furthermore the process was more sensitive to the airgap distance (needed to be kept small) when using IPA. The solvent dispersing in the coagulant during spinning was visible for water but not for IPA. Also more of the IPA than water followed the fibres up from the coagulation bath and was dripping from the rolls. The finished fibres coagulated and washed in IPA had a higher tendency of sticking to each other than those washed in water which in turn were sticking more than those coagulated in water. When handling, the fibres coagulated in IPA easily entangled and got kinked. A slightly more yellowish colour was observed after some time for the fibres coagulated and washed in IPA. Pictures of the different fibres can be seen in Appendix 4.

EmimAc has a higher affinity for water than IPA probably resulting in less solvent dissolved during the time the fibre is in the coagulation bath when using IPA. Most of the coagulation and recrystallization is instead likely to take place on the rolls and during the washing step. This could explain the higher tendency of the fibres to stick together. Another aspect is that the fabric softener used is meant for use in water and its interactions with IPA is not known. This could mean that the fibres washed in IPA have a different surface coating than the other types. The difference in maximum DR during spinning can also be explained by the difference in coagulation speed. If the cellulose is still mostly in solution there is no stable solid material to withstand the stretching but instead only solution sharing taking place and the fibre breaks.

Tensile testing

Mechanical properties for all types of regenerated cellulose fibres are summarised in Table 4 as the average of 10 measurements with standard deviation. Titer decrease with draw ratio but no tendency can be seen for the different preparation paths. Tenacity show a bigger dependence on preparation path than draw ratio and fibres coagulated and washed in water have an overall higher tenacity than those coagulated in IPA. The small change in tenacity with draw ratio falls within the standard deviation. Elongation for all types is slightly lowered with higher DR. Fibres coagulated and washed in IPA appears to have a higher elongation at break than the other types but it is still within the standard deviation.

Table 4. Mechanical properties and birefringence as average of ten measurements for all fibre types.

Draw Ratio	Coagulation bath	Washing bath	Titer [dtex]	Diameter [µm]	Tenacity [cN/tex]	Elongation [%]	Birefringence [Δn]
4	H_2O	H_2O	7.18 ±0.70	24.10 ±1.12	27.35 ±1.81	11.54 ±1.12	0.0401 ±0.0009
4	IPA	H_2O	7.25 ±0.86	23.64 ±1.53	20.01 ±1.74	12.02 ±2.37	0.0355 ±0.0021
4	IPA	IPA	7.32 ±1.38	26.13 ±2.06	14.76 ±1.97	16.53 ±5.17	0.0288 ±0.0026
6	H_2O	H_2O	5.39 ±0.75	19.27 ±2.00	29.99 ±2.76	10.28 ±0.83	0.0423 ±0.0008
6	IPA	H_2O	4.76 ±0.80	20.22 ±1.74	19.11 ±1.92	9.67 ±1.70	0.0358 ±0.0028
6	IPA	IPA	6.02 ±0.58	22.17 ±2.02	13.79 ±1.87	15.58 ±3.93	0.0304 ±0.0030

Even at a DR of 6 the resulting titer of 4-6 dtex is much larger than that of commercial fibres (1-2 dtex (Sixta et al. 2015)). To decrease this the DR would need to be increased beyond what the fibre hold for during spinning, alternatively an extruder with smaller holes could be tried. The larger tenacity for fibres coagulated in water suggest a higher crystallinity and/or higher level of orientation. This should also mean a lower level of elongation, since there is less material in the amorphous phase which can be stretched. However, it cannot be clearly determined from these results because of the large standard deviation. The higher elongation of fibres coagulated and washed in IPA inversely suggest a larger fraction of unordered amorphous phase. The decrease in elongation at higher DR for all fibres suggest more ordering of the chains and/or higher crystallinity. A larger change in DR is probably necessary to draw any conclusion and more fibres would need to be tested to decrease the standard deviation. Fibres from the very start and ending of the spinning session are likely to have different properties than the rest due to manual handling and if one of these happens to be tested it can highly affect the average obtained.

The obtained tenacity is comparable with the lower values for viscose and cotton in Table 2. Especially the fibres coagulated in water show signs of being able to reach commercially usable strength. The elongation at break is comparable to viscose and lyocell and slightly higher than that of cotton.

Birefringence

Birefringence and diameter for all regenerated cellulose fibres are summarised together with mechanical properties in Table 4 as the average of 10 measurements with standard deviations. The given diameter is calculated from the measured titer of those cellulose fibres on which birefringence was measured (not the same 10 fibres as tested for mechanical properties). It therefore appears to vary in a different way than the titer values in Table 4 but the difference falls within the standard deviation. It is clear that the diameter decrease with higher draw ratio. Birefringence seems to slightly increase with draw ratio but it is only for fibres coagulated in water that the difference exceeds the standard deviation. Again, it would be interesting to see the result for a larger change in DR. Fibres coagulated in water show higher birefringence than those coagulated in IPA also indicating higher crystallinity and/or ordering as concluded from the tensile testing by the higher strength.

Similar values of birefringence have been reported for fibres regenerated from NMMO and for the so called Ioncell-F fibres but in that case at much higher DRs (Sixta et al. 2015). This suggests that the cellulose chains in EmimAc has a higher tendency to order with less influence from stretching than in

some other solvents. The lower birefringence of fibres coagulated in IPA suggest that the ordering of the chains has to be fixed by crystallisation during the drawing state and that the chains relax on the rolls or during washing if this is not the case.

WAXS and SAXS - Fibre structure

Two dimensional WAXS patterns for all fibre types are seen in *Figure 14* a-f). The x-direction is defined as perpendicular to the fibre and the z-direction as parallel to the fibre. Small diffraction spots (at q_x around ±0.6 Å^{-1} and q_z ±1.2 Å^{-1}) are clearly visible for the fibres coagulated and washed in water (a) and d)) whereas a larger azimuthal broadening is seen for the fibres coagulated in IPA and washed in water (b) and e)). The presence of diffraction spots show that both of these types of fibres contain oriented and ordered crystalline domains. By comparison to previously indexed patterns, the scattering pattern has been identified as originating from cellulose II. For the fibres coagulated and washed in IPA (c) and f)) no real diffraction spots can be identified but the pattern is highly anisotropic. For all fibre types, only a small difference is seen between the different draw ratios but there is a slightly lower intensity and lower azimuthal broadening.

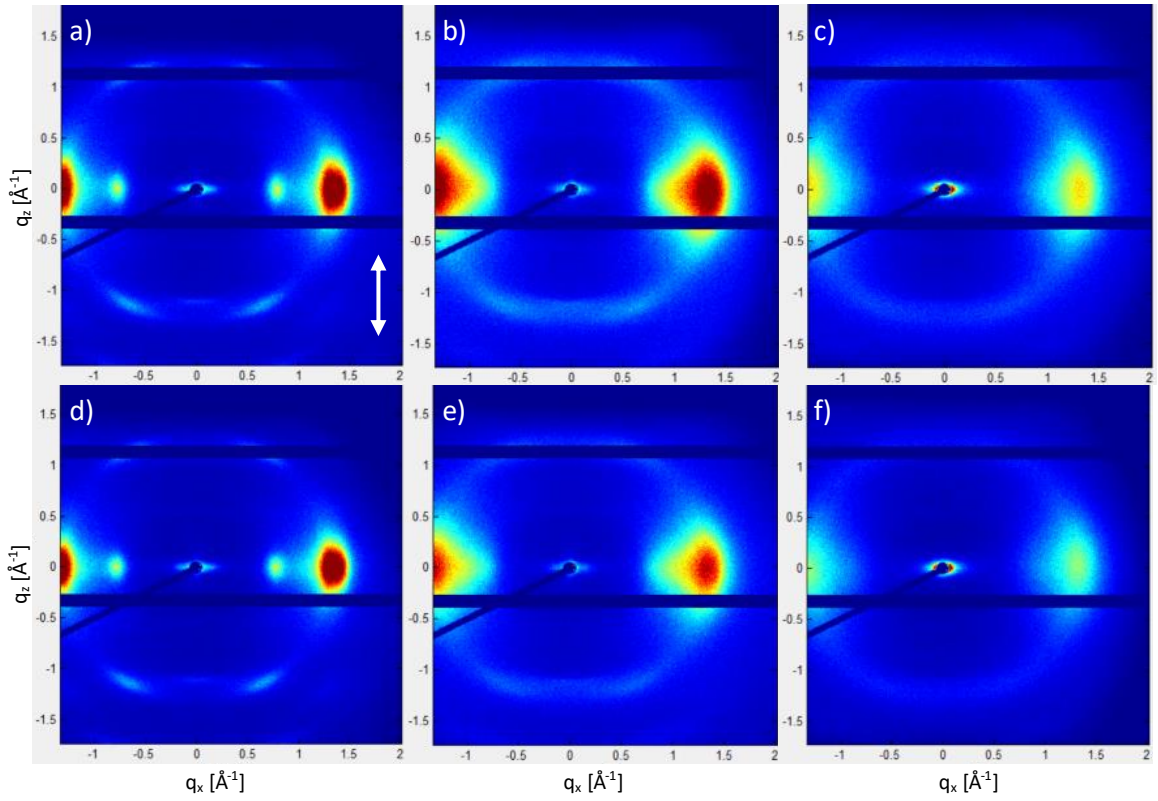

Figure 14. 2D WAXS patterns for fibres prepared in a) H_2O-H_2O, b) IPA-H_2O, c) IPA-IPA at DR=4 and d) H_2O-H_2O, e) IPA-H_2O, f) IPA-IPA at DR=6. The orientation of the fibres is indicated by the arrow in a).

Two dimensional SAXS patterns for all fibre types are seen in Figure 15 a-f). The x and z-direction is defined in the same way as for the WAXS patterns. All patterns show anisotropy with scattering mainly in a cross along the equatorial and meridional direction (perpendicular and parallel to the fibre axis). Again the fibres coagulated and washed in IPA (c) and f)) show the biggest difference with less sharp edges and more of a diffuse halo around the main scattering pattern. Very little difference is seen between the different draw ratios.

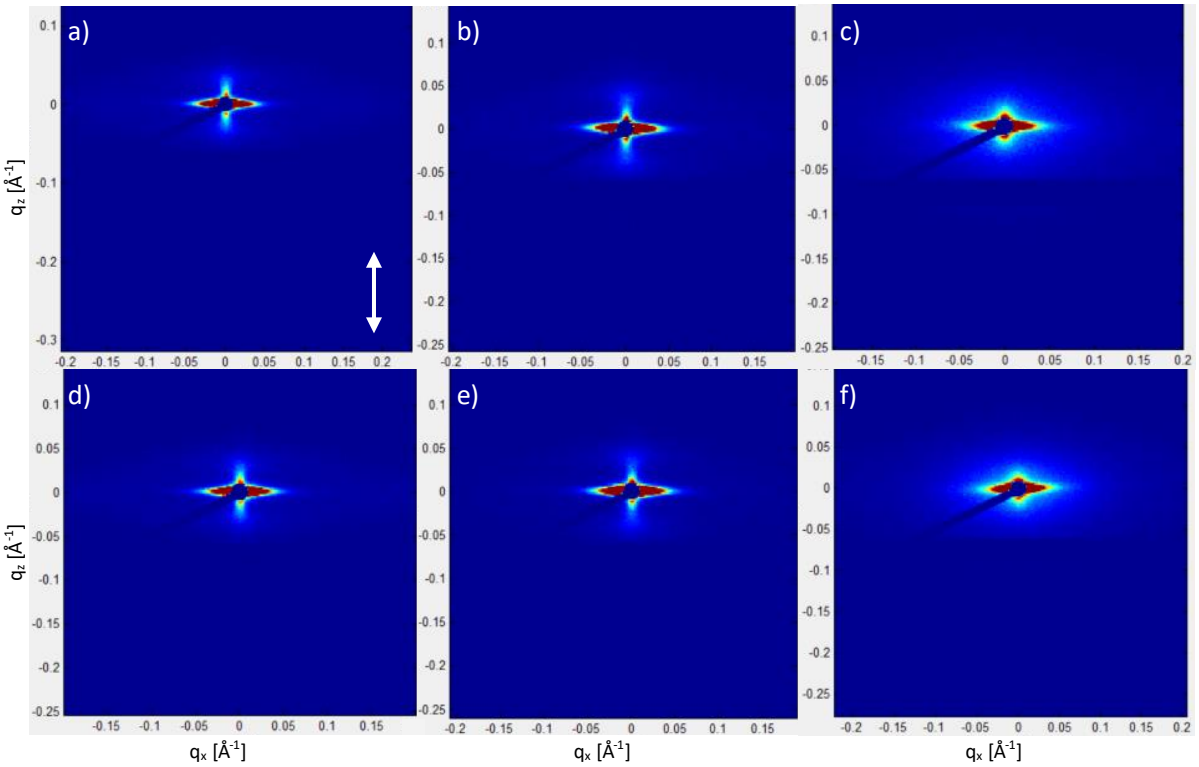

Figure 15. 2D SAXS patterns for fibres prepared in a) H_2O-H_2O, b) IPA-H_2O, c) IPA-IPA at DR=4 and d) H_2O-H_2O, e) IPA-H_2O, f) IPA-IPA at DR=6. The orientation of the fibres is indicated by the arrow in a).

The scattering in the equatorial direction is thought to originate from structures that are effectively infinite in the direction parallel to the fibre axis but have a finite size perpendicular to the fibre, like when considering a diffraction pattern resulting from a single slit experiment. Likewise, the scattering along the meridional direction is considered to arise from structures that are finite in the direction parallel to the fibre axis but infinite in the perpendicular direction. To further investigate these structures Figure 16 a-f) show 1D integrations of the SAXS data over 3° along the equatorial and meridional directions respectively. The scattering patterns differ slightly for the different preparation paths but more pronounced between the different directions. The same intensity is seen for the equatorial and meridional directions respectively for all fibre types even if different numbers of fibres were used. This is thought to be due to the x-ray beam having a smaller diameter (µm range) than the fibre bundles (mm range) so the same amount of fibres are exposed in each sample. Again no direct difference can be seen for the different draw ratios.

The equatorial scattering show a higher intensity than the meridional indicating a larger difference in electron density variations for the originating structures. A power law of q^{-4} can be determined for the major part of the q-range. This decay is interpreted as the slope of the Porod regime and indicates a sharp interface between the areas of different electron densities. There is no sign of a change in slope at lower q-values indicating that the structures responsible for the equatorial scattering have a radius much larger than $1/q_{min}$. The equatorial scattering is therefore considered to originate from the periodicity of the fibres themselves. The small hump seen in a) and d) at q=0.2 indicate some kind of internal structure at the size scale of 3 nm. What kind of structure this originate from is unknown but it could for example be micro-voids.

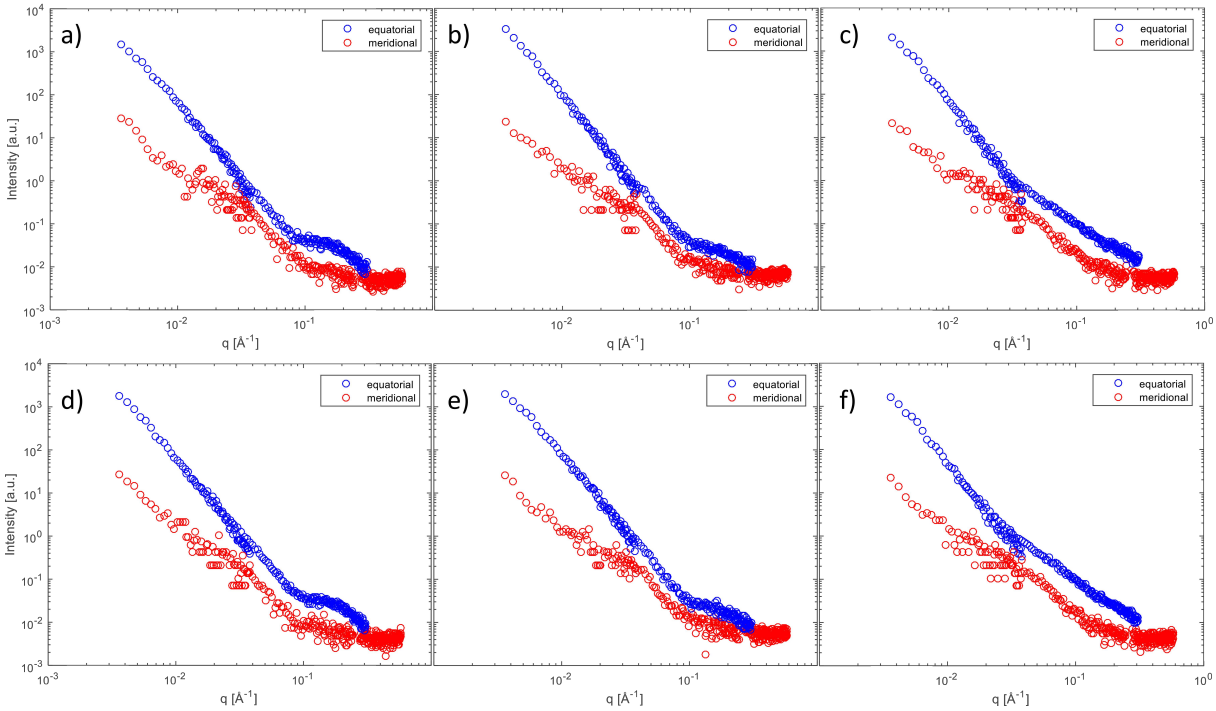

Figure 16. 1D SAXS patterns integrated along the equatorial (blue) and meridional (red) direction respectively from fibres prepared in a) H_2O-H_2O, b) IPA-H_2O, c) IPA-IPA at DR=4 and d) H_2O-H_2O, e) IPA-H_2O, f) IPA-IPA at DR=6.

The meridional scattering follow a power law of q^{-2} at low q changing to q^{-4} at q=0.03. This is considered as the start of the Porod regime and the previous q^{-2} dependence is interpreted as originating from a lamellar shape. The change in slope at q=0.03 is interpret as a lamella having a thickness (t) of 20 nm. No indication of a Guinier regime is seen at low q so the radius (r) of the lamellar cannot be determined but it is larger than the resolution limit. Polymers are known to crystallise in lamellar structures with chains meandering in and out of many different crystallites (Lindner and Zemb 2002) and the meridional scattering is therefore considered to originate from ordered cellulose crystallites. Figure 17 summarise the structure of the regenerated cellulose fibres described above with lamellar crystallites ordered along the length of the fibre and surrounded by an amorphous matrix.

Looking at the two dimensional WAXS and SAXS patterns, the fibres coagulated and washed in IPA appears less crystalline than the other types. There is not such a big difference seen in the one dimensional SAXS patterns but the transition from q^{-2} to q^{-4} is not as pronounced and the hump at q=0.2 is completely absent. These results agree with the conclusion from the birefringence and tensile testing.

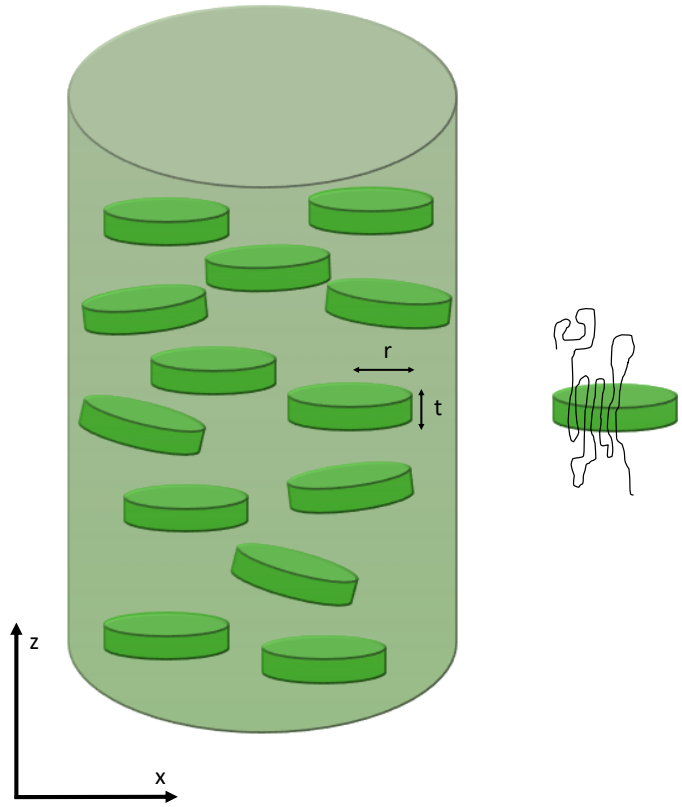

Figure 17. Schematic illustration of the proposed fibre structure with oriented lamellar crystallites of radius r and thickness t. The crystallites are composed of meandering polymer chains that can involve in many different crystallites along its length. The crystallites are surrounded by an amorphous matrix.

Conclusion and Outlook

Within the scope of this thesis work, cellulose was dissolved in the ionic liquid EmimAc and fibres were successfully spun from the solutions using air-gap spinning. The aim was to investigate alternative textile fibres with properties resembling cotton. Direct dissolution studies of MCC in EmimAc/DMSO showed a solubility limit of $n_{IL}/n_{AGU}\approx3$. More tests would be necessary to determine it more precisely and it would also be interesting to see if the same limit apply independent of the cellulose molecular weight. Through diffusion NMR measurements, it was evaluated that 1-1.5 acetate ions bind to each AGU in the DMSO diluted solvent. A value of 3 was expected based on the dissolution results but no explanation for this difference could be confirmed. Further evaluation of the number of bound ions at higher cellulose concentrations would be needed. In pure EmimAc, a structure of repeating anions and cations is considered to form around the cellulose chain because of electrostatic attraction and it could not be determined how many acetate ions that actually bind to each AGU. WAXS measurements would be needed to further analyse this structure. Fitting of the SAXS data show a stiff cylinder with a persistence length longer than the resolution limit which means a sterically hindered chain agreeing with the idea of an ionic structure. Furthermore, it could be concluded from the SAXS measurements that the cellulose chain behaves in the same way in the solvent independent of molecular weight. Repulsive interactions between the chains can be simulated with a structure factor according to equation 14.

As preparation for the fibre spinning, complex viscosity and cross over point was determined for a number of cellulose concentrations and temperatures. A solution of 15 wt% at 50°C was finally used for spinning because it showed the best agreement with the desired parameters. Further studies of the rheological properties of MCC and pulp respectively in EmimAc could be performed to lay the basis for further conclusions concerning the optimal spinning solution. Fibres of cellulose II were obtained at draw ratios of 4 and 6 with coagulation in water or IPA. Different coagulation mediums were compared because they are thought to affect the crystallinity of the fibre and thereby the mechanical properties. The spinning process was more sensitive during coagulation in IPA. Titer, diameter and elongation decreased slightly with higher draw ratio, birefringence increased. Together with the 2D WAXS and SAXS patterns this indicates a slightly higher crystallinity or at least more ordered chains at higher DR. A larger difference in DR and higher values tested is need to further evaluate this. It could though be hard to obtain such fibres as the values tested here were close to the maximum DR before breakage under the current conditions. Evaluation of more than 10 fibres is also needed to lower the standard deviation and obtain more reliable values.

The coagulation and washing medium showed a larger effect on the obtained fibre crystallinity than the draw ratio. Summarising the results from the mechanical testing and the 2D WAXS and SAXS patterns it becomes clear that coagulation and/or washing in water leads to a more ordered fibre structure than coagulation in IPA. This also show that the regeneration process does not stop after the coagulation bath but continues until the solvent is completely removed. This is helpful information when developing a procedure for retrieving the solvent. If a fibre with high crystallinity is required, IPA can still be used as coagulation medium if further washing is done with water. Of course this has the trade of that some of the solvent is lost in the water.

From the 1D SAXS patterns integrated over the equatorial and meridional directions, the idea of a fibre structure with 20 nm thick crystalline lamella surrounded by an amorphous matrix, as schematically shown in Figure 17, was developed. This structure differs from the recognised model of regenerated cellulose fibres containing different amounts of micro-voids but agrees too well with the data to assume differently. Since the equatorial scattering is assumed to originate from the periodicity of the

fibres themselves it would be interesting to see the pattern obtained if SAXS/WAXS was performed on one single fibre. Maybe this could help to further map out the inner structure in the parallel direction.

None of the fibres produced during the work of this thesis fulfil the criterions to be used in commercial applications. Primarily they need to be thinner, something that should be possible to obtain by trimming of the spinning parameters. Which fibre type is the best is impossible to say without knowing a specific application. A high solubility limit for cellulose, chemical stability and low spinning temperature are all factors that speak in favour of EmimAc as a cellulose solvent when producing regenerated cellulose fibres. Problems such as retrieving the solvent from the coagulation bath and obtaining equivalent properties in large scale production still needs to be solved. What can be said is that this is a very promising technique with many opportunities for further development. Developing sustainable and renewable materials for the textile industry is a question that has to be solved within a near future and it is not a utopia that people may walk around in clothing made from wood pulp and EmimAc.

References

Asaadi S, Hummel M, Ahvenainen P, Gubitosi M, Olsson U, Sixta H (2018) Structural analysis of Ioncell-F fibres from birch wood Carbohydr Polym 181:893-901 doi:10.1016/j.carbpol.2017.11.062

Bengtsson J (2016) Evaluating recyclability and suitability of tetrabutylammonium acetate:dimethyl sulfoxide as a solvent for cellulose. Master Thesis, Universiteit Gent

Budtova T, Navard P (2016) Cellulose in NaOH-water based solvents: a review Cellulose 23:5-55 doi:10.1007/s10570-015-0779-8

Callaghan PT (1991) Principles of nuclear magnetic resonance microscopy. Clarendon Press, Oxford University Press, Oxford England, New York

The Fibre Year (2017).

Fried JR (2009) Polymer science and technology. 2nd edn. Prentice Hall,

Gentile L, Olsson U (2016) Cellulose-solvent interactions from self-diffusion NMR Cellulose 23:2753-2758 doi:10.1007/s10570-016-0984-0

Gubitosi M, Duarte H, Gentile L, Olsson U, Medronho B (2016) On cellulose dissolution and aggregation in aqueous tetrabutylammonium hydroxide Biomacromolecules 17:2873-2881 doi:10.1021/acs.biomac.6b00696

Hedlund A (2013) Air gap spinning of cellulose fibers from ionic solvents. Master Thesis, Chalmers University of Technology

Hedlund A, Kohnke T, Theliander H (2015) Coagulation of EmimAc-cellulose solutions: dissolution-precipitation disparity and effects of non-solvents and cosolvent Nord Pulp Pap Res J 30:32-42

Hedlund A, Köhnke T, Theliander H (2017) Diffusion in Ionic Liquid–Cellulose Solutions during Coagulation in Water: Mass Transport and Coagulation Rate Measurements Macromolecules 50:8707-8719 doi:10.1021/acs.macromol.7b01594

Hu XP, Hsieh YL (1997) Breaking elongation distributions of single fibres J Mater Sci 32:3905-3912 doi:Doi 10.1023/A:1018656530385

ICAC, FAO (2015) Measuring sustainability in cotton farming systems. Food and Agriculture Organization of the United Nations, International Cotton Advisory Committee,

Idström A et al. (2017) On the dissolution of cellulose in tetrabutylammonium acetate/dimethyl sulfoxide: a frustrated solvent Cellulose 24:3645-3657 doi:10.1007/s10570-017-1370-2

Isik M, Sardon H, Mecerreyes D (2014) Ionic Liquids and Cellulose: Dissolution, Chemical Modification and Preparation of New Cellulosic Materials Int J Mol Sci 15:11922-11940 doi:10.3390/ijms150711922

Jackson AJ (2013) Introduction to Small-angle Neutron Scattering and Neutron Reflectometry. In.

Jiang GS, Huang WF, Li L, Wang X, Pang FJ, Zhang YM, Wang HP (2012) Structure and properties of regenerated cellulose fibers from different technology processes Carbohyd Polym 87:2012-2018 doi:10.1016/j.carbpol.2011.10.022

Kalliala EM, Nousiainen P (1999) Environmental profile of cotton and polyester-cotton fabrics AUTEX Research Journal 1:8-20

Klemm D, Heublein B, Fink HP, Bohn A (2005) Cellulose: fascinating biopolymer and sustainable raw material Angew Chem Int Ed Engl 44:3358-3393 doi:10.1002/anie.200460587

Kosan B, Michels C, Meister F (2008) Dissolution and forming of cellulose with ionic liquids Cellulose 15:59-66 doi:10.1007/s10570-007-9160-x

Le KA, Rudaz C, Budtova T (2014) Phase diagram, solubility limit and hydrodynamic properties of cellulose in binary solvents with ionic liquid Carbohydr Polym 105:237-243 doi:10.1016/j.carbpol.2014.01.085

Lindner P, Zemb T (2002) Neutrons, X-rays, and light : scattering methods applied to soft condensed matter. North-Holland delta series,, 1st edn. Elsevier, Amsterdam ; Boston

Lovell CS, Walker A, Damion RA, Radhi A, Tanner SF, Budtova T, Ries ME (2010) Influence of Cellulose on Ion Diffusivity in 1-Ethyl-3-Methyl-Imidazolium Acetate Cellulose Solutions Biomacromolecules 11:2927-2935 doi:10.1021/bm1006807

Maeda A, Inoue T (2011) On the Viscoelastic Segment Size of Cellulose Nihon Reoroji Gakk 39:159-163 doi:DOI 10.1678/rheology.39.159

Mezger TG (2014) The Rheology Handbook 4th Edition. Vincentz Network, Hanover

BNID110368 (2010) http://bionumbers.hms.harvard.edu/bionumber.aspx?&id=110368. Accessed 2018-03-15

Navard P, Wendler F, Meister F, Bercea M, Budtova T (2012) Preparation and Properties of Cellulose Solutions. In: The European Polysaccharide Network of Excellence (EPNOE). pp 91-152. doi:10.1007/978-3-7091-0421-7_5

Olsson C, Hedlund A, Idstrom A, Westman G (2014) Effect of methylimidazole on cellulose/ionic liquid solutions and regenerated material therefrom J Mater Sci 49:3423-3433 doi:10.1007/s10853-014-8052-3

Pusey PN (2002) Introduction to scattering experiments. In: Lindner P, Zemb T (eds) Neutrons, X-rays and Light. Elsevier Science B.V., University of Edinburgh, pp 3-21

Ries ME, Radhi A, Keating AS, Parker O, Budtova T (2014) Diffusion of 1-ethyl-3-methyl-imidazolium acetate in glucose, cellobiose, and cellulose solutions Biomacromolecules 15:609-617 doi:10.1021/bm401652c

Rieter Rikipedia. http://www.rieter.com/de/rikipedia/articles/rotor-spinning/applications-engineering/fiber-properties/fiber-tenacity-and-fiber-elongation/. Accessed 05-02 2018

SasView 4.1.2 Documentation. http://www.sasview.org/docs/user/models/flexible_cylinder.html. Accessed 10-04 2018

Schnablegger H, Singh Y (2011) The SAXS guide - Getting acquainted with the principles. Anton Paar, Austria

Sigma-Aldrich 1-Ethyl-3-methylimidazolium acetate. https://www.sigmaaldrich.com/catalog/product/aldrich/689483?lang=en&region=SE. Accessed 16/3 2018

Sigma-Aldrich Dimethyl sulfoxide. https://www.sigmaaldrich.com/catalog/product/sial/276855?lang=en&region=SE. Accessed 16/3 2018

Sixta H et al. (2015) Ioncell-F: A High-strength regenerated cellulose fibre vol 30.

Stejskal EO, Tanner JE (1965) Spin Diffusion Measurements: Spin Echoes in the Presence of a Time-Dependent Field Gradient The Journal of Chemical Physics 42:288-292 doi:10.1063/1.1695690

Stilbs P (1987) Fourier transform pulsed-gradient spin-echo studies of molecular diffusion Prog Nucl Mag Res Sp 19:1-45 doi:Doi 10.1016/0079-6565(87)80007-9

UN (2017) World Population Prospects: The 2017 Revision, Key Findings and Advance Tables. Department of Economic and Social Affairs, Population Division,

Vinogradova YS, Chen JY (2015) Micron- and nano-cellulose fiber regenerated from ionic liquids The Journal of The Textile Institute 107:472-476 doi:10.1080/00405000.2015.1040693

Appendix 1. Dissolution

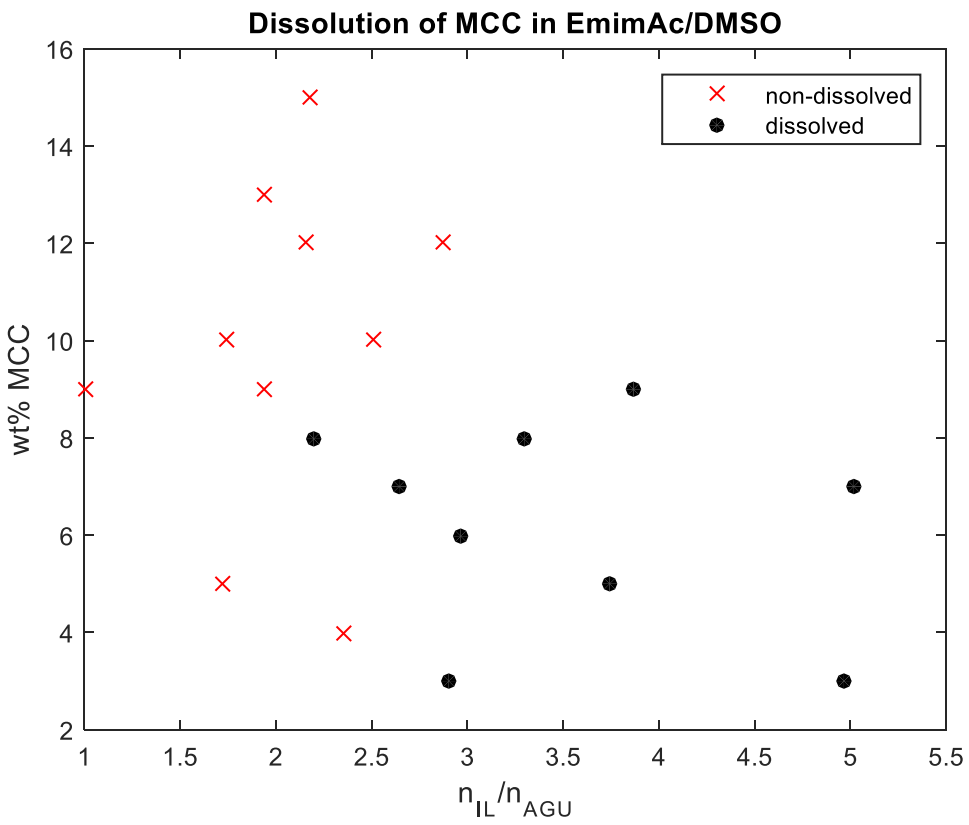

Figure 18. Solubility of MCC in EmimAc/DMSO based on the stoichiometric ratio of n_{IL}/n_{AGU}.

Appendix 2. Diffusion coefficients

Table 5. Diffusion coefficients for samples of MCC in EmimAc

Cellulose concentration [wt%]	Diffusion coefficient Ac^- [m^2/s]	Diffusion coefficient Cation [m^2/s]
0	$1.270 \cdot 10^{-11}$	$1.493 \cdot 10^{-11}$
0.5	$1.214 \cdot 10^{-11}$	$1.435 \cdot 10^{-11}$
1	$1.160 \cdot 10^{-11}$	$1.371 \cdot 10^{-11}$
2	$9.978 \cdot 10^{-12}$	$1.187 \cdot 10^{-11}$
3	$8.999 \cdot 10^{-12}$	$1.084 \cdot 10^{-11}$
4	$8.361 \cdot 10^{-12}$	$1.014 \cdot 10^{-11}$
5	$7.502 \cdot 10^{-12}$	$9.186 \cdot 10^{-12}$
10	$3.781 \cdot 10^{-12}$	$4.912 \cdot 10^{-12}$

Table 6. Diffusion coefficients for samples of MCC in 10 wt% EmimAc/DMSO

Cellulose concentration [wt%]	Diffusion coefficient Ac^- [m^2/s]	Diffusion coefficient Cation [m^2/s]	Diffusion coefficient DMSO [m^2/s]
0	$4.065 \cdot 10^{-10}$	$3.381 \cdot 10^{-10}$	$6.846 \cdot 10^{-10}$
1	$3.329 \cdot 10^{-10}$	$3.254 \cdot 10^{-10}$	$6.302 \cdot 10^{-10}$
2	$2.840 \cdot 10^{-10}$	$2.733 \cdot 10^{-10}$	$6.028 \cdot 10^{-10}$
3	$2.389 \cdot 10^{-10}$	$2.853 \cdot 10^{-10}$	$5.680 \cdot 10^{-10}$
3.5	$2.252 \cdot 10^{-10}$	$2.578 \cdot 10^{-10}$	$5.617 \cdot 10^{-10}$

Table 7. Diffusion coefficients for samples of MCC in 20 wt% EmimAc/DMSO

Cellulose concentration [wt%]	Diffusion coefficient Ac^- [m^2/s]	Diffusion coefficient Cation [m^2/s]	Diffusion coefficient DMSO [m^2/s]
0	$3.002 \cdot 10^{-10}$	$2.752 \cdot 10^{-10}$	$5.275 \cdot 10^{-10}$
1	$2.555 \cdot 10^{-10}$	$2.384 \cdot 10^{-10}$	$4.998 \cdot 10^{-10}$
2	$2.240 \cdot 10^{-10}$	$2.111 \cdot 10^{-10}$	$4.718 \cdot 10^{-10}$
3	$1.848 \cdot 10^{-10}$	$1.832 \cdot 10^{-10}$	$4.337 \cdot 10^{-10}$
4	$1.765 \cdot 10^{-10}$	$1.755 \cdot 10^{-10}$	$4.284 \cdot 10^{-10}$
5	$1.592 \cdot 10^{-10}$	$1.625 \cdot 10^{-10}$	$4.099 \cdot 10^{-10}$
6	$1.376 \cdot 10^{-10}$	$1.472 \cdot 10^{-10}$	$3.815 \cdot 10^{-10}$
7	$1.217 \cdot 10^{-10}$	$1.363 \cdot 10^{-10}$	$3.714 \cdot 10^{-10}$
8	$1.079 \cdot 10^{-10}$	$1.252 \cdot 10^{-10}$	$3.444 \cdot 10^{-10}$
9	$9.306 \cdot 10^{-11}$	$1.138 \cdot 10^{-10}$	$3.231 \cdot 10^{-10}$

Appendix 3. Matlab script

```
% Scattering from cylinders.
%***** INPUT ***************
cMCC = 0.01;        % cellulose concentration [g/ml] for 1% MCC
densityAGU = 1.5;   % cellulose mass density [g/ml]
sldMCC = 1.36e11;   % cellulose scatteringlength density [cm^-2]
Rc =4;              % Cylinder radius [Å]
L = 10000;          % Cylinder length [Å]

% ************************
q = 0.01:0.001:1;   % q-range [Å^-1]
sldEMIMAc =9.45e10; % solvent scattering length density
scale=1e-3;         %scale to make teory and exp data overlap

%**** Fibril (cylinder) scattering ****************
phiP=cMCC/densityAGU;
fun = @(X)
sin(X).*((sin(0.5*q.*L.*cos(X))./(0.5*q.*L.*cos(X))).*besselj(1,q.*Rc.*sin(
X))./(q.*Rc.*sin(X))*2).^2;
Y = integral(fun,0,pi/2,'ArrayValued',true);
Vc = 1e-21*L*pi*Rc^2;           % Cylinder volume
deltasld=sldMCC-sldEMIMAc;

Ic = phiP*deltasld^2*Vc*Y;

%*****Experimental data***
%Read from workspace: scattering_from_cylinder180213workspace
%                     SAXS180208workspace


%****Plotting****
loglog(q,Ic.*scale,'b-',q22,cIpulp1,'ko')   %q22 i Å^-1
xlabel('q [Å^-^1]')
ylabel('I(q) [cm^-^1/ wt%]')


%***Structure factor***
ny=30;              %excluded volume
S=1./(1+ny.*Y);
Is=Ic.*scale.*S;
hold on
loglog(q,Is,'r--');
legend('P(q)','Data pulp 1wt%','P(q)S(q)');
title('Pulp 1 wt%');
```

Appendix 4. Fibres

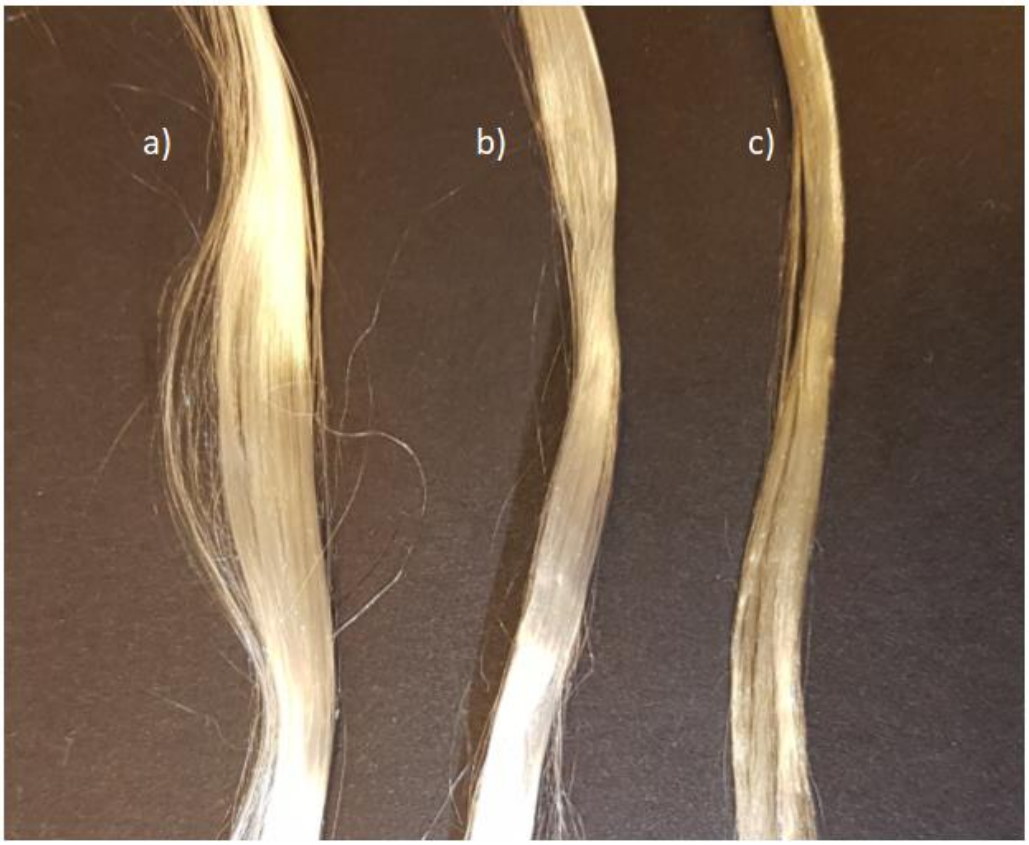

Figure 19. Picture of fibres prepared in a) H_2O-H_2O, b) IPA- H_2O and c) IPA-IPA at DR4.